

Characteristics of the Northern Hemisphere Warm Season Tropopause-Level Jet and Associated Trends

by

Libby J. Orr

A thesis submitted in partial fulfillment of
the requirements for the degree of

Master of Science

Department of Atmospheric & Oceanic Sciences

at the

University of Wisconsin - Madison

2024

Thesis Declaration and Approval

I, Libby J. Orr, declare that this Thesis titled ‘Characteristics of the Northern Hemisphere Warm Season Tropopause-Level Jet and Associated Trends’ and the work presented in it are my own.

Libby J. Orr		
_____	_____	_____
Author	Signature	Date

I hereby approve and recommend for acceptance this work in partial fulfillment of the requirements for the degree of Master of Science:

Jonathan Martin		
_____	_____	_____
Committee Chair	Signature	Date

Angela Rowe		
_____	_____	_____
Faculty Member	Signature	Date

Stephanie Henderson		
_____	_____	_____
Faculty Member	Signature	Date

Abstract

One of the most familiar structural features of Earth's atmosphere are the tropopause-level wind speed maxima known as jet streams or jets. These jets can be separated into two main types based on their differing means of formation. The polar jet arises as a result of eddy momentum flux convergence associated with developing waves within the region of midlatitude baroclinicity whereas the subtropical jet emerges in response to angular momentum transport from the Hadley Cell circulation. These jets are seasonally variable in both intensity and location. In the Northern Hemisphere, these two jets are assumed to exist throughout the full calendar year. This study aims to identify Northern Hemisphere warm season (April - November) tropopause-level jet streams based on their physical characteristics and to evaluate whether the two jet structure characteristic of winter persists into the warm season.

In this study, a calendar-year analysis of the isentropic housing of Northern Hemisphere tropopause-level jets is undertaken using the JRA-55, ERA5, and NCEP reanalysis datasets from 1979 - present. The analysis recreates a result of Christenson et al. (2017) which clearly shows a bimodal distribution of jet frequency of occurrence in the Northern Hemisphere cold season (November – April) with the two peaks corresponding to the polar and subtropical jets, respectively. The investigation uniquely reveals that the vast majority of the warm season (May – October) is characterized by a unimodal distribution suggestive of a single tropopause-level jet during these months. Furthermore, the waviness of this warm season unimodal tropopause-level jet is considered from the perspective of the average latitudinal displacement (ALD) diagnostic of Martin (2021). Trends in waviness, speed, and latitudinal location of the unimodal jet over 60-plus year and 41-year time periods are also calculated. While results vary across data sets, the

unimodal jet does seem to be getting wavier over the full 61-year period while exhibiting no clear trend in speed and no significant trend in latitudinal location. Over the 41-year time span, only trends in jet speed lack consensus as only two of the three data sets suggest that the jet has slowed with time.

Acknowledgements

I would first like to thank my advisor, Jon Martin, for taking me on as a graduate student and trusting me to research such an engaging subject. I have been able to grow as a researcher, writer, teacher, and scientist through your continued support and am now a more confident scientist than my undergraduate self thought possible. I would also like to thank my committee members, Angela Rowe and Stephanie Henderson, for their guidance and expertise during the process of completing my master's research and thesis.

I wouldn't have been able to make it through the first years of grad school and everything else that goes along with getting a master's degree if it hadn't been for the close group of friends I've made in my time at UW. Whether by our trivia Tuesdays, the many movie nights at each other's apartments, or the couple of trips up north, you all have made the hard classes seem easier and the stressful days feel lighter. Similarly, the graduate student cohort, faculty, and staff of AOS have all made this department so welcoming. Moving to Wisconsin was made a lot easier because of all of you, and I couldn't have asked for a better place to end up.

A huge thank you goes to my fellow Martin lab mates, Patrick, Poush, and Flora. You all have been with me from the very beginning and on every step of the way to me getting this degree. Our office has always been a fun and inviting place and I wouldn't have enjoyed my time here nearly as much if it weren't for all the good times we have in the office and our many volleyball games. I know that as long as I have you guys in the office, I'll have someone to confide in, a place to rant, someone to trust, and people I can call my very best friends. Patrick, you have had my back since before I was even officially a grad student here. I wouldn't be where I am now without your constant support, encouragement, and coding help (even though you hate

xarray). I'm glad I've gotten to have you with me for the first few years of grad school and will have you for the many more challenges to come.

Finally, I would like my family for everything they've done to help support me and get me this far in both my education and life. As my education progressed I kept moving northward, and you all were with me every step of the way. To my mom, Michele, my dad, Joey, and my brother, Nick, thank you for the numerous trips up north to visit and the lifelong encouragement to go as far as I possibly can in life. You instilled a love of science and education in me from the very beginning and have done so much to make sure I could pursue my dreams. I don't have room here to list everyone, but the rest of my family has always been there supporting me the entire time as well, and I couldn't thank you all enough (hopefully all the cheese I bring home makes us almost even). A special thank you goes to my grandpa, Papa Orr, who passed before he could see me finish my master's degree, but always made sure to let me know that I "got all my smarts" from him.

This work is supported by NSF grant #AAJ6543.

Table of Contents

Abstract	ii
Acknowledgements	iv
Table of Contents	vi
List of Figures	vii
List of Tables	xii
Chapter 1 - Introduction	1
1.1 <i>Introduction to Jet Streams</i>	1
1.2 <i>Identifying Jet Streams</i>	3
1.3 <i>Jet Streams In A Warming Climate</i>	5
Chapter 2 - Data & Methodology	10
2.1 <i>Data</i>	10
2.2 <i>Isentropic Distribution</i>	11
2.3 <i>Average Latitudinal Displacement</i>	12
Chapter 3 - Results	19
3.1 <i>Calendar Year Climatology of Northern Hemisphere Jet Distribution</i>	19
3.2 <i>Warm Season Jet Waviness Trends</i>	22
3.3 <i>Warm Season Jet Speed Trends</i>	23
3.4 <i>Warm Season Jet Equivalent Latitude</i>	24
3.5 <i>41-Year Climatology</i>	25
Chapter 4 - Summary and Discussion	44
Bibliography	55

List of Figures

Figure 2.1: The frequency of occurrence of qualifying grid columns with a maximum wind speed value within the specified 5-K isentropic layers for the month of January, from the JRA-55 dataset. The 310–325-K and 340–355-K layers are shaded in blue and red, respectively. Percentage of grid columns belonging to each shaded layer is also represented.

Figure 2.2: An example of wind speeds (shading) in the 335 – 350 K layer and the corresponding core isertel (black contour) for June 15, 1995, as depicted by the JRA-55 dataset. The physical meaning of, and method for determining, the core isertel are described in the text. For this particular day and layer the core isertel has a value of 2.5 PVU.

Figure 2.3: Frequency of occurrence of core isertel value for each reanalysis dataset during the Northern Hemisphere warm season (May - October). The dashed vertical lines indicate the mean PV value of the core isertel from each data set. Isertel values given in potential vorticity units (PVU, $1 \text{ PVU} = 10^{-6} \text{ K m}^2 \text{ kg}^{-1} \text{ s}^{-1}$).

Figure 2.4: Schematic illustrating the meridional displacements of the core isertel from its equivalent latitude from June 15, 1995, using the JRA-55 data set. The equivalent latitude on this day has a value of 34.9° N and is highlighted by the red dashed circular

contour. Poleward and equatorward displacements are highlighted as well, in bright red contours and blue contours, respectively.

Figure 3.1: A calendar-year climatology of the Northern Hemisphere jet distribution as depicted by the JRA-55 dataset. The polar and subtropical jets are represented by blue and red columns, respectively, while the single warm season jet is denoted in purple (Jan. - Jun.).

Figure 3.1 (continued): (Jul. – Dec.)

Figure 3.2: The NCEP portrayal of the jet stream distribution transition from bimodality to unimodality in the month of April, signaling the start of the warm season (May - October). The y-axis is presented at a smaller scale than in prior histogram figures to better depict the modality transition.

Figure 3.3: The NCEP portrayal of the jet stream distribution transition from unimodality back to bimodality in the month of November, signaling the start of the cold season (Dec. – Mar.). The y-axis is presented at a smaller scale than in prior histogram figures to better depict the modality transition.

Figure 3.4: An overlay of the jet distributions for the months of January and July as seen in the NCEP dataset. The warm season unimodal jet (purple) overlaps a portion of the cold season subtropical jet (red) in isentropic space.

Figure 3.5: A calendar-year climatology of the Northern Hemisphere jet distribution as depicted by the ERA5 dataset. The polar and subtropical jets are represented by blue and red columns, respectively, while the single warm season jet is denoted in purple (Jan. - Jun.).

Figure 3.5 (continued): (Jul. – Dec.)

Figure 3.6: A calendar-year climatology of the Northern Hemisphere jet distribution as depicted by the NCEP dataset. The polar and subtropical jets are represented by blue and red columns, respectively, while the single warm season jet is denoted in purple (Jan. – Jun.).

Figure 3.6 (continued): (Jul. – Dec.)

Figure 3.7: Seasonal average ALD (in degrees) of the unimodal warm season jet (May - October). Each of the colors represents a different reanalysis time series. The straight black line through each time series represents the trend line (taken from the JRA-55 data) for each. The trend line exhibits a significant trend for the ERA5 and NCEP datasets.

Figure 3.8: Average wind speed (m s^{-1}) along the core isertel of the warm season (May - October) unimodal jet. Each of the colors represents a different reanalysis time series. The straight black line represents the trend line for the JRA-55 dataset. Over the time

series, ERA5 exhibits a significant decrease in wind speeds whereas NCEP displays a significant increase in wind speeds.

Figure 3.9: Seasonal average equivalent latitude of the unimodal warm season (May - October) jet. Each of the colors represents a different reanalysis time series. The straight black line through each time series represents the trend line (taken from the JRA-55 data) for each. The trend line does not exhibit a significant trend for any dataset.

Figure 3.10: Seasonal average ALD of the warm season (May - October) unimodal jet confined to the satellite era (1979 - 2019). Each of the colors represents a different reanalysis time series. The straight black line through each time series represents the trend line (taken from the JRA-55 data) for each. ALD is increasing at a significant rate in the ERA5 and NCEP data sets only.

Figure 3.11: Average wind speed (m s^{-1}) of the warm season (May - October) unimodal jet core confined to the satellite era (1979 - 2019). Each of the colors represents a different reanalysis time series. The straight black line through each time series represents the trend line (taken from the JRA-55 data) for each. Wind speeds are significantly decreasing in the JRA-55 and ERA5 data sets while NCEP data exhibits no significant trend.

Figure 3.12: Average equivalent latitude of the warm season (May - October) unimodal jet confined to the satellite era (1979 - 2019). Each of the colors represents a different

reanalysis time series. The straight black line through each time series represents the trend line (taken from the JRA-55 data) for each. All three data sets exhibit relatively weak slopes and have no significant trends.

Figure 4.1: The JRA-55 data set's depiction of the unimodal to bimodal jet distribution transition in the month of November for the years 1959 – 1988. The lower overall count of columns is an artifact of shortening the examined timescale.

Figure 4.2: The JRA-55 data set's depiction of the unimodal to bimodal jet distribution transition in the month of November for the years 1989 – 2019. The lower overall count of columns is an artifact of shortening the examined timescale.

List of Tables

Table 3.1: Isentropic housings of the polar, subtropical, and unimodal jet streams over the course of a calendar year for all three reanalysis datasets. Layers highlighted in red indicate those which are not the same across all datasets. Only 6 of 54 layers do not match, meaning 88% of all selected layers are identical.

Chapter 1

Introduction

1.1 Introduction to Jet Streams

Among the most common features of Earth's atmosphere are the tropopause-level wind speed maxima known as jet streams or jets. These narrow streams of fast-moving air are a fundamental link between synoptic-scale weather systems and large-scale circulations around the globe. Since these jets play such a substantial role in production of weather phenomena in the mid-latitudes (e.g., Whitney 1977; Athanasiadis et al. 2010; Harnik et al. 2016), they have been the subject of numerous observational studies over time. The question of how these jets will change in a warming climate has become an active topic of discussion in recent years (e.g., Archer and Caldeira, 2008; Barnes & Polvani, 2013; Miller et al., 2006). In either hemispheres' cold season (JJAS for the Southern Hemisphere, DJFM for the Northern Hemisphere), there are two main jet streams that can be identified at any given time: the subtropical jet and the polar jet.

As established in Held & Hou (1980), the subtropical jet arises in response to angular momentum transport from the thermally direct Hadley Cell circulation. As such, the subtropical

jet resides at the poleward edge of the Hadley Cell, at $\sim 30^\circ$ latitude in the upper troposphere (~ 200 hPa). The polar jet sits atop the baroclinicity of the midlatitudes, usually located north of $\sim 40^\circ$ latitude at around 300 hPa (Namias and Clapp 1949; Newton 1954; Palmén and Newton 1969; Keyser and Shapiro 1986; Shapiro and Keyser 1990). This jet, often called the eddy-driven jet, forms as a result of eddy momentum flux convergence associated with developing waves within this region of midlatitude baroclinicity (Held 1975; Rhines 1975; McWilliams and Chow 1981; Panetta 1993).

As a result of their means of formation, the polar and subtropical jets are generally separated both latitudinally and vertically. The jets are seasonally variable, exhibiting changes in both intensity and location throughout the year. During wintertime, the Northern Hemisphere has jet stream maxima generally located over the western Pacific, adjacent continental Asia, and the western Atlantic. The summer months are characterized by less extensive wind speed maxima overall which are generally located over the western Atlantic and the western to central Pacific (Koch et al. 2006). Occasionally during the Northern Hemisphere extended cold season (November - March), these two jets can become vertically superposed, resulting in a single feature characterized by much faster wind speeds (Christenson et al. 2017). Despite the substantial attention that has been devoted to examining the tropopause-level jets, prior studies have mainly focused on examining these jets in the cold season. Consequently, this thesis focuses on identification and assessment of the characteristics of the warm season tropopause-level jet and considers whether two separate jets exist throughout the full calendar year.

A defining characteristic of both species of jets is that they reside near the tropopause, a thermodynamic boundary separating the troposphere from the stratosphere. Importantly, the tropopause does not exist at one uniform height but instead slopes upward toward the equator.

Through observational work by Defant and Taba (1957), the Northern Hemisphere cold season tropopause was found to have a three-step structure in height from equator to pole with local regions of steep slope occurring at increasingly lower altitudes with increasing latitude. These sharp gradients in tropopause height were also found to be collocated with axes of local wind speed maxima, i.e. the jets. Furthermore, Defant and Taba (1957) established that, on average, the tropical tropopause was found to reside at ~ 90 hPa and extend to $\sim 30^\circ\text{N}$. At that latitude, tropopause height sharply decreases to ~ 200 hPa. This sharp break in tropopause height is coincident with the subtropical jet which is located at ~ 200 hPa. Poleward of this jet is the “middle tropopause”, located around ~ 250 hPa. Another tropopause break separates the middle tropopause from the even lower polar tropopause. The polar jet is located at this break, at ~ 300 hPa. These jets can also be characterized by their baroclinicity; shallow upper troposphere baroclinicity distinguishes the subtropical jet whereas the deep and dramatically more baroclinic polar front drapes below the polar jet.

The present research seeks to categorize the warm season tropopause-level jet stream based on its observed physical characteristics (i.e. location in isentropic space) rather than via rigid, pre-determined qualifications such as latitudinal location or specific pressure levels. In this way, a feature-based identification of the tropopause-level jet emerges that is less contingent upon preconceived bias than prior identification methods mentioned herein.

1.2 Identifying Jet Streams

To better characterize the location of the Northern Hemisphere tropopause-level jet stream, the present study examines the jet at its location on a “dynamic tropopause” rather than at a pre-ordained height or pressure level. Morgan and Nielsen-Gammon (1998) advocated for

the use of potential temperature (θ) and wind speed maps on the “dynamic tropopause” [defined as a surface of constant Ertel potential vorticity (PV) (Ertel 1942)] for diagnosing weather systems. When considered from this perspective, the steep tropopause breaks become regions of large PV gradient on isentropic (θ) surfaces, or large θ gradient on isertelic (constant PV) surfaces, linking them both theoretically (Cunningham and Keyser, 2004; Hoskins et al., 1985) and empirically (Davies and Rossa, 1998; Hoskins and Berrisford, 1988) to the tropopause-level jet cores. Cunningham and Keyser (2004) utilized quasi-geostrophic potential vorticity to relate tropopause-level PV gradients and jet maxima. Their theoretical methodology is discussed in detail in Chapter 2 of this thesis. Davies and Rossa (1998) offered evidence for this concept in an empirical sense through their examination of upper-tropospheric fronts from a PV perspective. In their analysis, PV gradients were examined in both isobaric and isentropic vertical coordinates. Through their case study they suggested an alternative interpretation of frontogenesis as the enhancement of the PV gradient on isentropic surfaces. Furthermore, their cross sections indicated the co-occurrence of strong (and strengthening) PV gradients with an accompanying jet streak. Despite a growing acceptance of this θ /PV perspective on the tropopause-level jets, there is no clear consensus regarding which isentropic surfaces (or layers) are the most appropriate to house these jet-defining PV gradients. A number of studies (e.g. Defant and Taba 1957, Palmen and Newton 1969, Morgan and Nielsen-Gammon 1998, Shapiro et al. 1999, and Randel et al. 2007), however, suggest a relatively narrow range of acceptable values for these layers; 335K - 345K for the subtropical jet and 310K - 320K for the polar jet. This thesis follows the method devised by Christenson et al. (2017), to be fully discussed in later sections, who offered a method to empirically identify the appropriate layers. It has not yet been established whether or not, and

to what degree, these layers persist as the housings of the two species of tropopause-level jets throughout the Northern Hemisphere warm season (May - October).

A particularly influential study in jet stream identification is that of Koch et al. (2006). This analysis was one of the first to partition jet stream events into those with deep and shallow baroclinicity, exploiting one of the primary differences between the subtropical and polar jets. In order to be considered a jet stream event in their study, integrated average wind speeds in the 100 hPa to 400 hPa layer had to be greater than 30 m s^{-1} , a criterion which many subsequent studies have adapted as a basis for their jet identification schemes (e.g. Manney et al. 2011, 2014, 2017, Christenson et al. 2017, Manney and Hegglin 2018). In addition to this integrated wind speed specification, Christenson et al. (2017) also utilized the relationship between jet cores and sharp PV gradients to identify the separate types of jet streams, a concept that will be explored in depth in later sections. This method allowed for the separate objective identification of each type of jet, along with their respective isentropic housings.

1.3 Jet Streams In A Warming Climate

Given the importance of jet streams to global weather, it is of both operational and scientific interest to consider how these structures might evolve in a changing climate. Various different methods in previous analyses have been created to identify jet streams, determine their general locations, and assess their trends in a variety of characteristics such as wind speed and latitudinal location over time. As may be expected with differing methodologies, variable results and conclusions have been articulated. Archer and Caldeira (2008) utilized mass-weighted average wind speeds in the upper troposphere to characterize speeds, pressure levels, and latitudinal locations of jet streams in both hemispheres. They ultimately reached the conclusion

that, in both hemispheres, jet streams have shifted poleward and, in the Northern Hemisphere, weakened in intensity. Conversely, Strong and Davis (2007), through the use of wind speeds on a “Surface of Maximum Wind”, found that Northern Hemisphere jet streams are shifting equatorward while simultaneously increasing in core speed. Manney et al. (2011, 2014, 2017) and Manney and Hegglin (2018) identified jet streams by selecting regions in the upper troposphere in which there is a wind speed maximum greater than 40 m s^{-1} . The boundaries of these jet streams were considered to be wherever wind speeds drop below 30 m s^{-1} . If there were multiple areas above 40 m s^{-1} within the selected 30 m s^{-1} regions, jet cores could only be considered separate if they were 15° apart and were separated by winds less than 25 m s^{-1} . Employing this definition, they were able to create a jet climatology in both hemispheres across various data sets and found results that depict somewhat of a middle ground from those previously discussed. In the Northern Hemisphere, they found that the subtropical jet is moving poleward whereas the polar jet is both weakening and moving equatorward in our warming climate. Despite the widely variable methodologies of jet identification across studies utilizing reanalysis data, there is a surprising consensus, in studies that employ climate models, that both jets will trend poleward in a warming world in studies which employ climate models (e.g., Barnes & Polvani, 2013; Miller et al., 2006; Swart & Fyfe, 2012; Woollings & Blackburn, 2012; Yin, 2005).

Jet stream waviness is another characteristic that has been the subject of recent research efforts. Through its linkage to synoptic-scale weather systems, changes in jet stream waviness can trigger and lead to changes in daily weather extremes (Röthlisberger et al., 2016). As such, it is important to understand how jet waviness will evolve in a warming world. A variety of measures to calculate jet waviness have been developed in recent analyses. Some methodologies

utilize Fourier analyses of meridional winds and geopotential heights in select latitude bands to assess wave amplitudes (Petoukhov et al., 2013; Coumou et al., 2014; Screen and Simmonds, 2013, 2014). Most studies focus on the contribution of warming lower tropospheric temperatures at higher latitudes, also known as Arctic amplification, and their impacts on the tropopause-level jets (Blackport & Screen, 2020; Burt et al., 2016; Francis, 2017; Francis et al., 2018; Screen & Simmonds, 2010, 2013; Serreze et al., 2009; Vavrus, 2018). A majority of these analyses apply metrics that utilize geopotential height contours or horizontal wind components in the middle to upper troposphere (i.e. ~500 hPa) to characterize waviness of flow patterns (e.g., Barnes, 2013; Chen et al., 2015; Di Capua & Coumou, 2016; Francis & Vavrus, 2012, 2015; Martineau et al., 2017). When considered from a PV perspective, flow at 500 hPa is strongly influenced by near surface thermal contrasts (i.e., dynamically equivalent to low-level PV gradients following Bretherton, 1966), internal diabatic processes, and tropopause-level PV anomalies (Davis & Emanuel, 1991; Grams et al. 2011; Hoskins et al., 1985). So, though this 500 hPa flow often exhibits similarities to the tropopause-level jet stream patterns at high altitudes, it is still affected by these lower tropospheric and diabatic influences to a greater extent than the tropopause-level flow. Consequently, it may be expected that the tropopause-level jet waviness would differ from that of wind speed maxima in the mid-troposphere. As a result of the wide variety of analysis methodologies, there is little to no consensus on whether a warming world will be characterized by substantial changes in jet structure and waviness (Barnes, 2013; Barnes and Screen, 2015). Of most importance to this thesis is the research and methodology presented in Martin (2021), in which a robust methodology for assessing waviness of jet streams and their recent trends is provided. This procedure considers the polar and subtropical jets separately within their

respective isentropic housings, as in Christenson et al. (2017). An in-depth discussion of this methodology will be provided in a later section within this thesis.

Despite the numerous efforts to characterize jet stream behavior in a warming climate, little work has been done to study these distributions and trends during the warm season (May - October) alone. Several of the aforementioned research papers have focused mainly on their respective hemisphere's tropopause-level jet stream in the cold season, providing little insight into how these features behave throughout the remainder of the calendar year. Other studies (e.g., Archer and Caldeira, 2008; Barnes and Screen, 2015; Manney et al. 2011, 2014, 2017) examine trends of tropopause-level jet streams in all seasons. Each study views Northern Hemisphere jet streams in a unique way, such as viewing the jet as one long spiral covering the full hemisphere as seen in Archer and Caldeira (2008) or utilizing the Koch et al. (2006) standards along with latitude bounds as done in Manney et al. (2017). Some studies make no assumption about the classification of the jet (i.e. polar or subtropical) and solely study broad jet stream characteristics (e.g., Archer and Caldeira, 2008; Barnes and Screen, 2015). Others classify these jets with their own unique methodologies and focus on identifying the two jets and assessing their individual characteristics over a full year (e.g., Manney et al. 2011, 2014, 2017). No study, however, has been fully devoted to establishing the existence of a two jet structure and characterizing the traits of these jets trends in the warm season alone. The present research seeks to investigate aspects of the climatology and long term trends of the Northern Hemisphere warm season tropopause-level jets by identifying their isentropic location and then applying the waviness metric seen in Martin (2021) in three reanalysis datasets.

The thesis is organized as follows. Chapter 2 provides insight into the datasets used for the analysis and a description of the methodology used to objectively identify the isentropic

distribution of the subtropical and polar jets. A full description of the physical and observational aspects of the waviness metric developed by Martin (2021) is offered as well. Chapter 3 displays the results of the Northern Hemisphere warm season jet climatology, covering features such as distribution in isentropic space and trends of jet waviness, speed, and latitudinal location. Finally, Chapter 4 discusses the summary and conclusions of these findings, as well as providing insight for potential future work.

Chapter 2

Data & Methodology

2.1 Data

The ensuing analysis utilizes zonal (u) and meridional (v) winds as well as temperature (T) at 6 h intervals from three different reanalysis data sets: the Japanese 55-year reanalysis (JRA-55), the National Centers for Environmental Prediction/National Center for Atmospheric Research (NCEP/NCAR) reanalysis, and the European Centre for Medium-Range Weather Forecasts (ECMWF) Reanalysis v5 (ERA5). Sixty-one years of data from NCEP/NCAR reanalysis at 17 isobaric levels to 10 hPa on a 2.5° latitude-longitude grid (Kalnay et al. 1996; Kistler et al. 2001) from 1959 to 2019 were used. The JRA-55 data set was employed over the same 61 years (1959-2019) on 60 vertical levels up to 0.1 hPa on a horizontal grid mesh of ~ 55 km (Kobayashi et al. 2015). Lastly, the ERA5 data on 137 vertical levels from the surface to 80 km with a grid spacing of 31 km covering the 41-year time period of 1979-2019 (Copernicus Climate Change Service [CS3], 2017) was also used. The different reanalyses are the products of varying assimilation schemes and input data sets, with some characterized by known

discontinuities arising from the introduction of satellite data (e.g., Santer et al. 1999; Sturaro, 2003). Additionally, the use of data sets with variable start times can complicate the comparison of any resulting time series. The foregoing analysis embraces these differences as evidence of, rather than impediments to, the robustness of the analysis method.

2.2 Isentropic Distribution

In order to assess waviness and various other characteristics of the warm season tropopause-level jet, it is first necessary to establish where the jet lies in isentropic space. To make this assessment, the present analysis follows aspects of those performed by Koch et al. (2006) and Christenson et al. (2017). Firstly, the maximum wind speed in each grid column of each data set (from 0°N to 80°N) is identified and the corresponding pressure (P_{max}) and potential temperature (θ_{max}) values at the level of maximum wind speed are identified. Following Koch et al. (2006), only the grid columns in which the integrated average wind speed between 400 hPa and 100 hPa is greater than 30 m s^{-1} are retained. From such qualifying columns in each data set, θ_{max} is sorted into 5 K bins for the purpose of constructing an isentropic distribution of the level of maximum wind for each month of the year.

An example of this is provided in Figure 2.1, which shows the 61-year isentropic distribution of January jet cores from the JRA-55 data. Three peaks stand out in this distribution: one in the 310 - 325 K layer, a sharper one in the 340 - 355 K layer, and a muted one in the 405 - 420 K layer. These peaks correspond to the polar jet, subtropical jet, and polar night jet, respectively. While the polar night jet is present in the cold season months' distributions, it is consistently located above the tropopause and will not be considered further in the subsequent analysis.

2.3 Average Latitudinal Displacement

Once the isentropic housings of the jet are established for each month, the Average Latitudinal Displacement (ALD) methodology, first established by Martin (2021), is employed to assess jet stream waviness. Following Cunningham and Keyser (2004), consideration of the quasi-geostrophic potential vorticity (QGPV) elucidates a direct relationship between PV gradients and strong jet cores. The QGPV is given by

$$(1) \quad q_g = \frac{1}{f_0} \nabla^2 \varphi + f + \frac{\partial}{\partial p} \left(\frac{f_0}{\sigma} \frac{\partial \varphi}{\partial p} \right) = \Lambda(\varphi) + f$$

(where $\Lambda = \frac{1}{f_0} \nabla^2 + \frac{\partial}{\partial p} \left(\frac{f_0}{\sigma} \right) \frac{\partial}{\partial p} + \frac{f_0}{\sigma} \frac{\partial^2}{\partial p^2}$ and φ is the geopotential). Consequently, the cross-jet gradient of QGPV $\left(\frac{\partial q_g}{\partial n} \right)$ can be written as

$$(2) \quad \frac{\partial q_g}{\partial n} = \Lambda \left(\frac{\partial \varphi}{\partial n} \right) = \Lambda(-fV_g)$$

after substituting in the expression for the geostrophic wind in natural coordinates. This relationship makes clear that large horizontal gradients of tropopause-level PV are collocated with local geostrophic wind speed maxima.

Given this relationship, it follows that the jet core will reside in a region of strong PV gradient. Thus, the axis of maximum wind speed of a jet can be approximated by one of several PV contours (isertels) within that strong PV gradient region. The specific isertel will hereafter be referred to as the “core isertel” as it refers to the core of the jet on any given day. To find this core isertel, the circulation, given by

$$(3) \quad C = \oint \vec{U} \cdot d\vec{l}$$

is calculated along each isertel ranging from 0.5 to 5 PVU ($1 \text{ PVU} = 10^{-6} \text{ m}^2 \text{ K kg}^{-1} \text{ s}^{-1}$) at 0.1 PVU intervals in each jet layer on every day in each data set. The isertel along which the circulation per unit length is maximized serves as the core isertel for that given day in that layer. An example of the core isertel in the 335 - 350 K isentropic layer from the JRA-55 data on June 15, 1995 can be seen in Figure 2.2.

Since identifying the core isertel on any given day involves assessment of the circulation, it also requires calculation of contour length. Consequently, fair comparison among the 3 data sets is only possible by adopting a uniform horizontal grid spacing. Therefore, all three data sets were bilinearly interpolated onto isentropic surfaces at 5 K intervals (from 300 to 370 K) at 2.5° latitude/longitude grid spacing. The particular isentropic layers used for the analysis were identified for each month according to the method just described and will be revealed in a subsequent chapter.

The core isertel is not the same for each day in a given time series nor for any given day that might be shared by two or more of the three time series. Consequently, its distribution in each data set is worthy of additional analysis. Figure 2.3 displays these distributions for the warm season (May - October) jet as seen in all three data sets. The NCEP data set exhibits a high concentration of lower PV values, with around 17% of all core isertels in the 61-year period having a value of around 1.9 PVU. The ERA5 and JRA-55 data sets are in more agreement with each other, both featuring a much broader distribution than seen in NCEP data. ERA5 core isertels have a mean value of 2.4 PVU, whereas JRA-55 core isertels exhibit a mean value of around 2.9 PVU, both values notably higher than their NCEP counterpart. Regardless of these various distribution differences, the mean core isertel value amongst all data sets has a relatively small range of 1.2 PVU.

Once the core isertel for a jet on a given day in a given layer is determined, the area enclosed within that isertel can be calculated. Next, a polar cap whose area is equal to that same area is calculated. The southern edge of this cap is the equivalent latitude of that core isertel and is given by

$$(4) \quad \phi_e = \arcsin \left[1 - \frac{A}{2\pi R_e^2} \right]$$

where R_e is the radius of the earth and A is the area enclosed by the core isertel. The meridional displacement of the core isertel from its equivalent latitude at each longitude in the data set can then be measured, as seen in Figure 2.4, which revisits the example from June 15, 1995. If an isertel intersects a longitude line multiple times, only segments of the longitude line along which the PV is greater (less) than the core isertel value south (north) of the equivalent latitude are counted. The sum of the length of all these qualifying segments is divided by the number of longitude lines at the resolution of the data (in this case, $2\pi/2.5^\circ = 144$) and converted to degrees, resulting in the final measure of Average Latitudinal Displacement (ALD). According to this procedure, a perfectly zonal core isertel (i.e., a zonal jet) would have an ALD of 0.0 with larger numbers representing increasingly wavier jets. Returning to the example case again, the core isertel in Figure 2.4 has an ALD value of 5.56°.

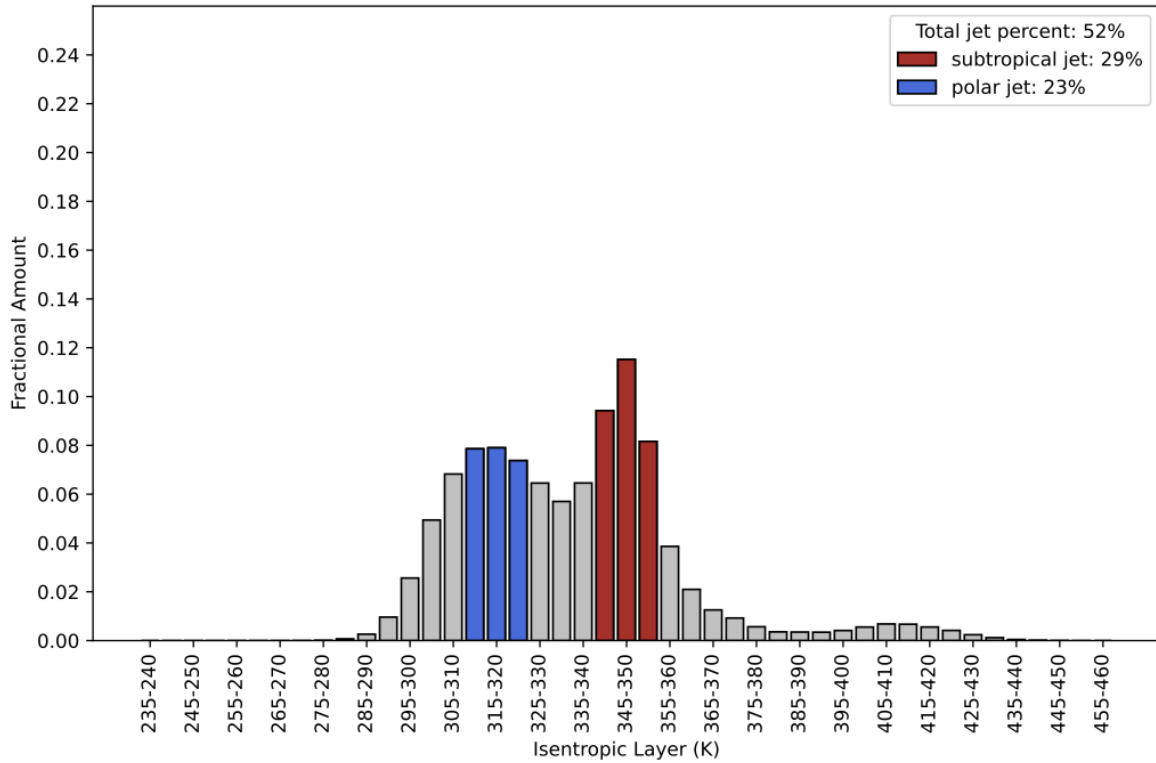


Figure 2.1: The frequency of occurrence of qualifying grid columns with a maximum wind speed value within the specified 5-K isentropic layers for the month of January, from the JRA-55 dataset. The 310–325-K and 340–355-K layers are shaded in blue and red, respectively. Percentage of grid columns belonging to each shaded layer is also represented.

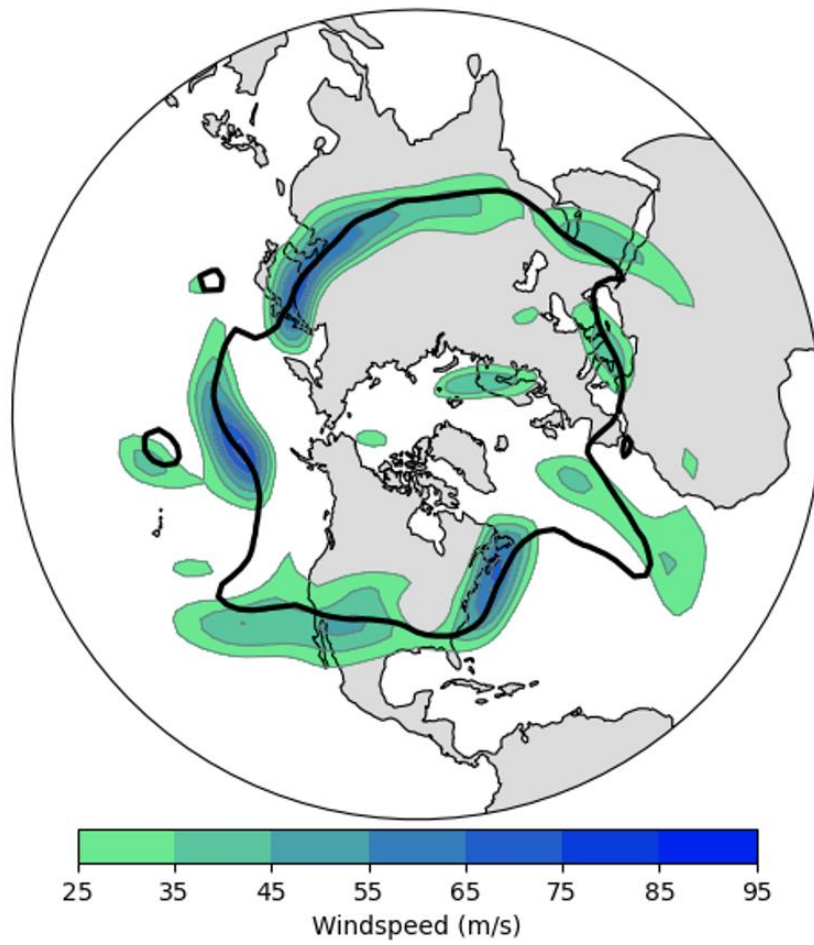


Figure 2.2: An example of wind speeds (shading) in the 335 – 350 K layer and the corresponding core isertel (black contour) for June 15, 1995, as depicted by the JRA-55 dataset. The physical meaning of, and method for determining, the core isertel are described in the text. For this particular day and layer the core isertel has a value of 2.5 PVU.

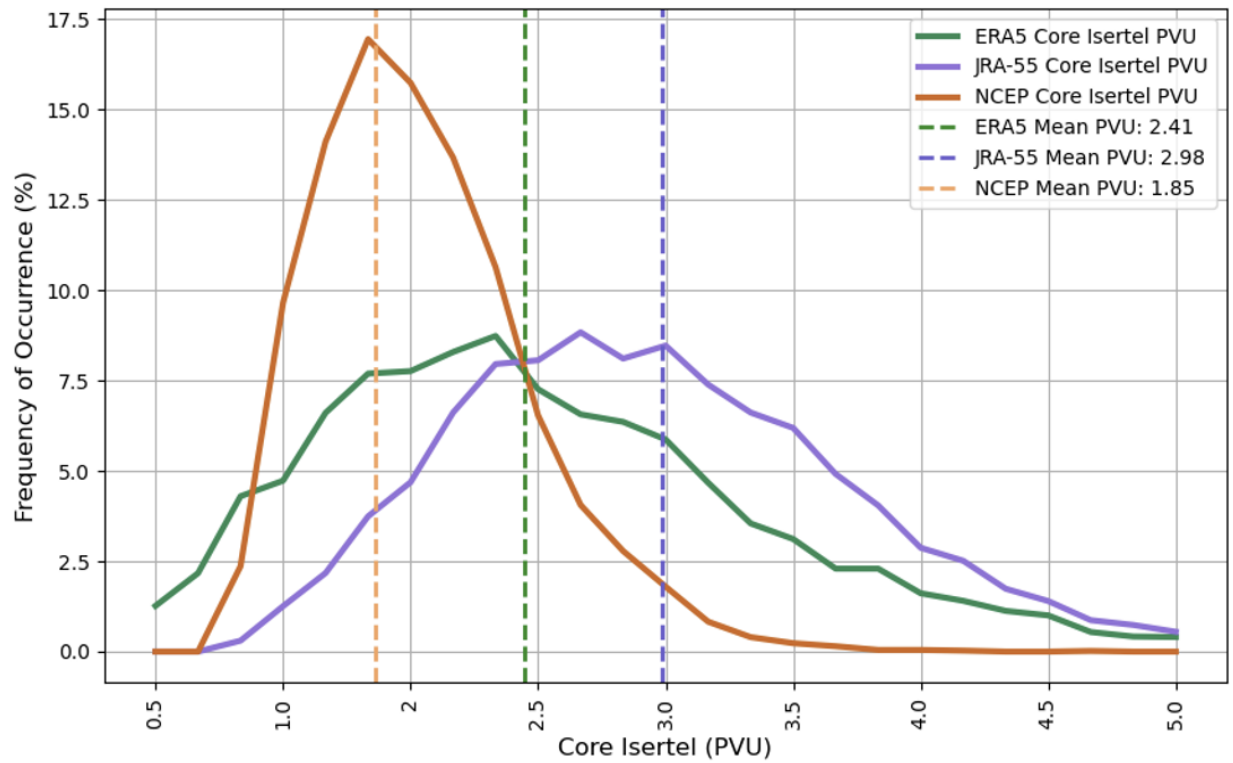


Figure 2.3: Frequency of occurrence of core isertel value for each reanalysis dataset during the Northern Hemisphere warm season (May - October). The dashed vertical lines indicate the mean PV value of the core isertel from each data set. Isertel values given in potential vorticity units (PVU, $1 \text{ PVU} = 10^{-6} \text{ K m}^2 \text{ kg}^{-1} \text{ s}^{-1}$).

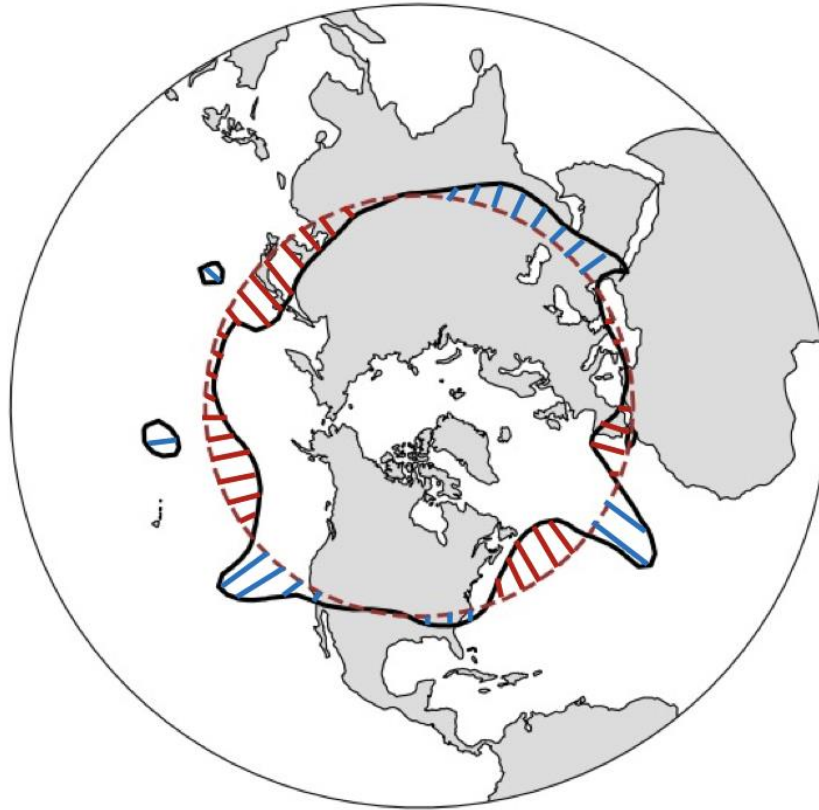


Figure 2.4: Schematic illustrating the meridional displacements of the core isertel from its equivalent latitude from June 15, 1995, using the JRA-55 data set. The equivalent latitude on this day has a value of 34.9° N and is highlighted by the red dashed circular contour. Poleward and equatorward displacements are highlighted as well, in bright red contours and blue contours, respectively.

Chapter 3

Results

3.1 Calendar Year Climatology of Northern Hemisphere Jet

Distribution

The isentropic distributions of the tropopause-level jet streams for each month during the Northern Hemisphere warm season are established in this portion of the analysis. The cold season distribution results from Christenson et al. (2017) are also recreated so that a full calendar year climatology of the θ -space jet distributions can be examined. Figure 3.1 displays this full climatology from the JRA-55 data set. A distinct pattern in jet distribution quickly becomes apparent; the warm season is dominated by a unimodal peak in the distribution whereas the cold season has two peaks, representing the distinct polar and subtropical jets, respectively.

The warm season months (May - October) are characterized by a smaller number of qualifying grid columns overall but with much more concentrated peaks in their distributions, meaning a high percentage of jet-containing columns fall into the single peak (Figs. 3.1 e - i). While the cold season does feature a higher number of qualifying columns and a wider

distribution, around half of all columns are still contained within the two chosen jet layers for all months (Figs. 3.1a - d, k and l). Christenson et al. (2017) adopted the 315 - 330 K and 340 - 355 K layers as the isentropic housings for the cold season polar and subtropical jet, respectively, as these were the peaks in the NCEP reanalysis jet distributions. The isentropic housings of the warm season unimodal jet are selected following the same convention to maintain continuity with the previous methodology. These housings fluctuate slightly throughout the course of the warm season. During May, the first month fully characterized by a unimodal jet, 330 - 345 K is the appropriate layer (Fig. 3.1e). The jet shifts to the slightly warmer 335 - 350 K layer for June (Fig. 3.1f), but returns to the 330 - 345 K layer for July - September (Figs 3.1g-i). To close out the warm season, October features the coolest unimodal jet of all, when it occupies the 325 - 340 K layer, though with a broader distribution than in any of the preceding 5 months (Fig. 3.1j). The percentage of jet-containing columns residing in the unimodal jet also fluctuates throughout the course of the warm season. May is occupied by a less defined unimodal jet which contains just below 50% of all qualifying grid columns. This percentage increases to well above half of all columns (up to 54% in Figure 3.1h) for the majority of the warm season before falling back to just under 40% in October, the last month with a fully unimodal jet.

April and November are transitional months in which the Northern Hemisphere jet transforms from a unimodal to bimodal distribution (November) or from a bimodal to unimodal (April). Partitioning April and November into 10-day average periods sheds more light on the nature of these transitions. Figure 3.2 illustrates the bimodal to unimodal transition that dominates April. The month starts out as fully bimodal, separate peaks for the polar and subtropical jet separated by a minimum in the distribution (Fig. 3.2a). This minimum is identified if at least one 5 K bin has a lower count of jet-containing columns than those

characterizing the adjacent peak(s). The intervening minimum becomes less prominent by April 10th (Fig. 3.2b) and is completely nonexistent by April 20th (Fig 3.2c). Finally, by April 30th, any signs of bimodality are gone and the distribution is distinctly unimodal (Fig. 3.2d), remaining that way throughout the extended warm season. In the early stages of this unimodal jet, fewer jet-containing columns reside within the selected isentropic range (around only 40%) despite the distribution being distinctly unimodal. By mid-warm season, however, this number increases to well over 50% as the unimodal jet becomes more well established.

The opposite transitional pattern unfolds in November, as demonstrated by Figure 3.3. The month begins with a solidly unimodal jet distribution, albeit with a wider distribution than in the late summer/early fall (Fig. 3.3a). The unimodal distribution persists through November 10th with continued broadening while the jet core maximum shifts to lower isentropic levels (Fig. 3.3b). By November 20th, two peaks separated by a minimum in the distribution emerge (Fig. 3.3c). These separate peaks become more clearly defined by November 30th (Fig. 3.3d) and persist through mid-April. Similar to its initial stages in April, the final stages of the unimodal jet are also characterized by fewer jet-containing columns, just above 30%, until its transition to bimodality. After this transition, the polar and subtropical jet layers contain over 50% of all qualifying columns.

The warm season unimodal jet resides in a rather unique isentropic space between where the cold season polar and subtropical jets are located. Figure 3.4 compares the jet distribution in January (mid-cold season) to July (mid-warm season) to better exhibit the stark differences between the two. In January, the polar jet occupies the 310 K - 325 K layer whereas the subtropical jet resides at the higher 340 K - 355 K level. The warm season unimodal jet occupies the 335 K - 350 K layer, placing it a slightly lower θ than the cold-season subtropical jet layer.

The slight overlap between the warm season unimodal jet layer and the cold season subtropical jet layer suggests that the polar jet erodes away during the warm season, weakening or disappearing while the subtropical jet layer takes over.

The other data sets were also analyzed with the same methodology to see if they contain the warm season unimodal jet pattern as well. Figures 3.5 and 3.6 show the year-long climatology for the ERA5 and NCEP data sets, respectively. Though very particular details of these companion distributions may differ, these figures, in addition to Figure 3.1, demonstrate that the broad details of the annual cycle of the tropopause-level jet stream(s) are remarkably similarly depicted in each of these distinct reanalysis data sets.

All three of the reanalysis data sets are in decent consensus regarding the isentropic location of each jet. Table 3.1 lists these calendar year isentropic housings for each data set with those housings not in agreement with the consensus highlighted in red. Only six isentropic layers do *not* match, meaning 88% of all isentropic housings across all three data sets *are* in agreement. Three of the six non-consensus layers reside in the NCEP data set, the least modern of the three. We will consider this fact later in the thesis.

3.2 Warm Season Jet Waviness Trends

Now that the isentropic housing of the unimodal jet has been established, its waviness can be assessed. The seasonal average of daily ALD for each data set is calculated over the full warm season (May - October). Figure 3.7 displays a time series of these results for each of the three reanalysis data sets. For this and each of the following characteristics' analyses, only the JRA-55 trendline is shown. The interannual variability exhibited in these time series, as well as the overall ALD values, are relatively similar across all data sets with NCEP being the largest

outlier, especially in the more recent portions of the time series where ALD values are $\sim 0.7^\circ$ higher (not shown). Significance of the trend for each data set was evaluated using a two-sided Student's t-test. The JRA-55 trendline has a p-value of 0.38, which is not significant, while having a slope of 0.002. The lack of significance to this modest slope suggests the warm season jet's ALD has been relatively constant over this time period, staying around 7.3° .

Conversely, the ERA5 time series depicts the unimodal jet getting modestly wavier with time. While not displayed in Figure 3.7, the ERA5 trendline has a slope of 0.009 and a p-value of 0.0001, meaning its increase in waviness of around 0.3° is significant at the 95th percentile. The NCEP data set has a strongly significant increase in jet ALD of about 0.5° over the 61-year time period, with a p-value of 5.2×10^{-5} and a slope of 0.01. These stark differences further establish the NCEP data set as an outlier in this half of the analysis as well.

3.3 Warm Season Jet Speed Trends

The core isertel was previously defined as the isertel along which circulation per unit length is maximized. Consequently, it is safe to assert that the average wind speed along that core isertel represents the average jet speed on that day. The time series of seasonal average (May - October) speed for each data set is portrayed in Figure 3.8. While all data sets have a similar average relative speed of the jet core over time, around $22 - 23 \text{ m s}^{-1}$, long-term trends are more variable with this characteristic than with others. JRA-55 data maintains average jet wind speeds at around 22.5 m s^{-1} with some fluctuations over the time series. However, with a slope of 0.002 and a p-value of 0.35, no significant trend is present. NCEP data exhibits wind speeds that are slightly weaker than those in the other two data sets as well as average speeds that increased noticeably within the first 20 years of the time series but flattened out in the latter

portion. Overall, NCEP features a modest but statistically significant increase in average wind speed of around 0.5 m s^{-1} over time, featuring a trendline slope of 0.008 and a p-value of 0.02. Conversely, ERA5 data depicts a unimodal jet that has steadily slowed by about 1 m s^{-1} with time. This data set has both the most defined slope at a value of -0.022 and the most significant p-value at 0.0002.

3.4 Warm Season Jet Equivalent Latitude

Another useful by-product of finding the core isertel is that the daily values of equivalent latitude fall right out of the analyses. The equivalent latitude is very nearly the zonally averaged latitude of the jet core on any given day. The time series of the seasonal average equivalent latitude (May - October) for the unimodal jet for each data set is shown in Figure 3.9. Similar to what was seen in the trends of previously examined unimodal jet characteristics in the JRA-55 dataset, no significant change is exhibited ($p = 0.51$) over time. The warm season unimodal jet is neither moving poleward or equatorward at a significant rate but has generally remained in the same relative location latitudinally between 40°N and 41°N . This is the only characteristic for which all three data sets agree on overall lack of trend significance, with NCEP and ERA5 trendlines having p-values of 0.55 and 0.97 respectively. Despite this agreement, overall values are still notably different between data sets. ERA5 places the unimodal jet slightly more equatorward than JRA55 with it residing generally between 39°N and 40°N . As seen in the prior characteristics' analyses, NCEP is the largest outlier of the three datasets. It portrays a much more poleward unimodal jet, placing it around 42.5°N for the majority of the time series.

3.5 41-Year Climatology

Reanalysis data sets that incorporate data from satellite observations are often thought to be the most accurate. Starting in 1979, various new satellites were able to acquire higher quality observations from all latitudes (Kobayashi et al. 2015; Bell et al. 2020), allowing for more accurate representations of the atmospheric state in reanalysis data sets. Within the present analysis, only the JRA-55 and ERA5 data sets were assimilated with these satellite observations whereas NCEP, prior to 1979, was not. Given this, each of the previously examined unimodal jet characteristics are reassessed in the 1979 - 2019 time span in an effort to discern if any trends differ in this modern satellite era.

Figure 3.10 shows the ALD time series in this smaller time span. Both NCEP and ERA5 data still depict the unimodal jet becoming significantly wavier with time, featuring about a 0.5° and a 0.4° increase respectively. The NCEP time series has featured a p-value of 0.003 while ERA5 had a p-value of 0.0001. JRA-55 data, however, shows no significant trend and remains around 7.15° for the entirety of the time frame. It is worth noting that, while still significant, the NCEP trendline's p-value is 0.004, a value that is much larger in this 41-year time period than over its original 61-year timeframe.

The most drastic change in significance occurs in the core isertel wind speed time series seen in Figure 3.11. Previously, none of the data sets agreed with one another and only the ERA5 dataset depicted a unimodal jet that slowed with time. In this more recent and restricted time frame, JRA-55 data now also portray a unimodal jet that slows by around 0.5 m s^{-1} with a slope of -0.01 and a p-value of 0.04, an important difference from its former lack of any significant trend. JRA-55 and ERA5 are much more similar in this smaller time frame as both data sets now feature around a 0.5 m s^{-1} slowing of the unimodal jet over the 41-year time period. In this

limited period even the NCEP data set depicts little change in wind speeds as it has a slightly negatively sloped trend line with an insignificant p-value of 0.6.

Finally, Figure 3.12 displays the 41-year time series of the unimodal jet's equivalent latitude. Much like its 61-year counterpart, none of the data sets in this time period feature a significant trend in equivalent latitude. NCEP and JRA-55 data sets are the most similar, both featuring very similar peaks and troughs in their time series, but overall remaining around 40.5°N. NCEP portrays a unimodal jet that, despite its many fluctuations, hovers around a latitude around 42.5°N, occasionally reaching values of up to 3° poleward of the other datasets.

The NCEP data set trends are notably different from the others displayed in this analysis, portraying values that are overall higher or lower than those in the JRA-55 or ERA5 data sets both before and during the satellite era. Despite these differences, all three data sets follow the same general pattern of peaks and troughs in their respective interannual variabilities. One potential reason for this discrepancy is differences in the spatial and temporal resolutions of the data sets used. The ERA5 has improved representation of convective updrafts, gravity waves, and other meso- to synoptic-scale features that can enhance mixing due to its higher spatial and temporal resolutions. The NCEP and JRA-55 data sets, however, have lower resolutions that likely curtail such mixing and may, therefore, underlie these differences (Hoffman et al. 2019). Additionally, Xu et al. (2021) found similar issues when utilizing the NCEP, JRA-55, and ERA-Interim reanalysis data sets to examine climatic and seasonal averages of vertical motions in the atmosphere over China. They found that the JRA-55 and ERA-Interim data sets similarly represented both the magnitude and distribution of vertical motion centers while the NCEP data often portrayed substantial distribution differences, and occasionally opposite values, as compared to the more modern datasets. They concluded that, while positions of vertical motion

centers were relatively the same across all data sets, the magnitude and spatial distribution of these centers were the most similar between ERA-Interim and JRA-55 data sets. NCEP data often portrayed results that were generally different from or even opposite values of those seen in the other two data sets.

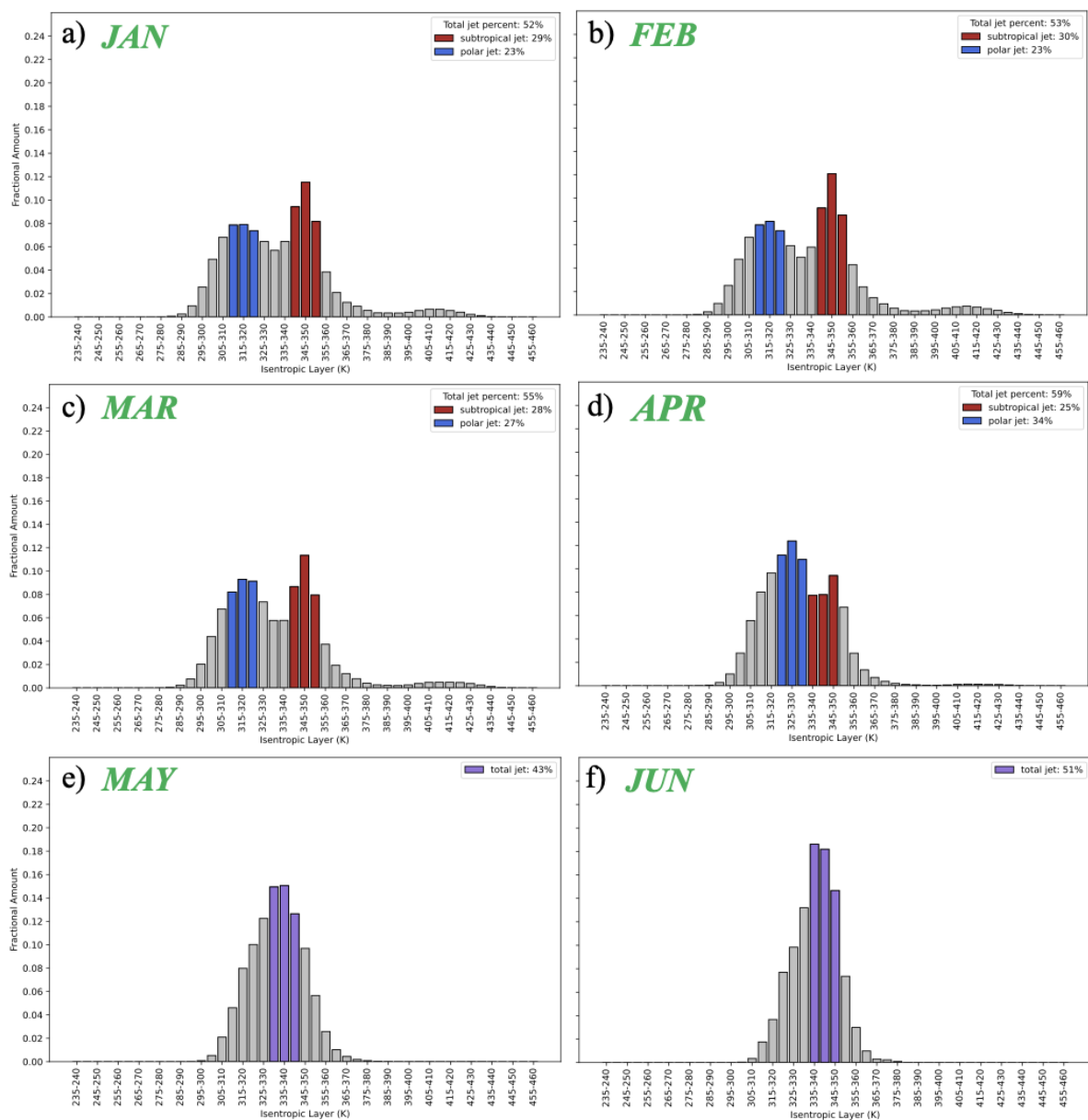


Figure 3.1: A calendar-year climatology of the Northern Hemisphere jet distribution as depicted by the JRA-55 dataset. The polar and subtropical jets are represented by blue and red columns, respectively, while the single warm season jet is denoted in purple (Jan. - Jun.).

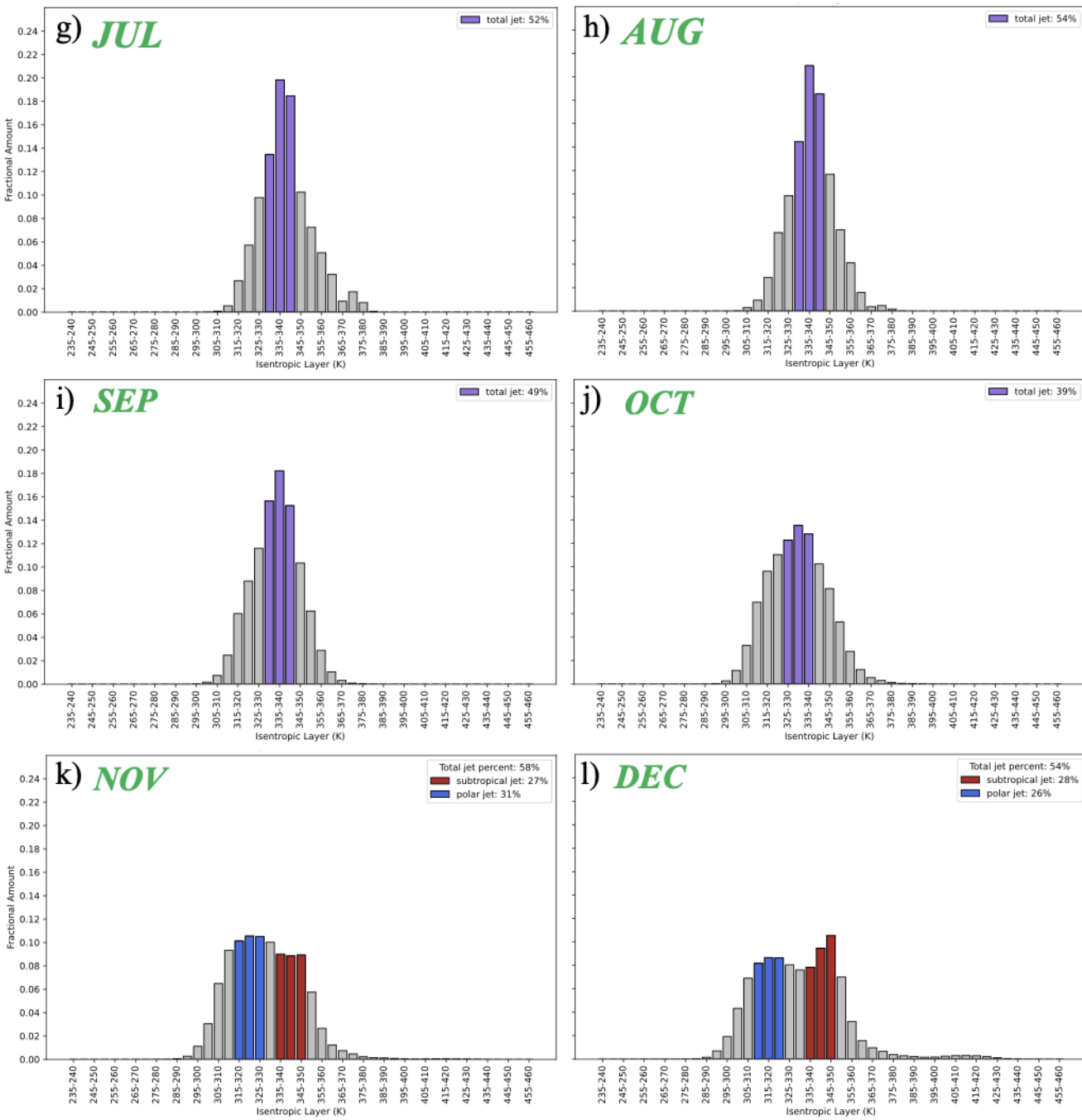


Figure 3.1 (continued): (Jul. – Dec.)

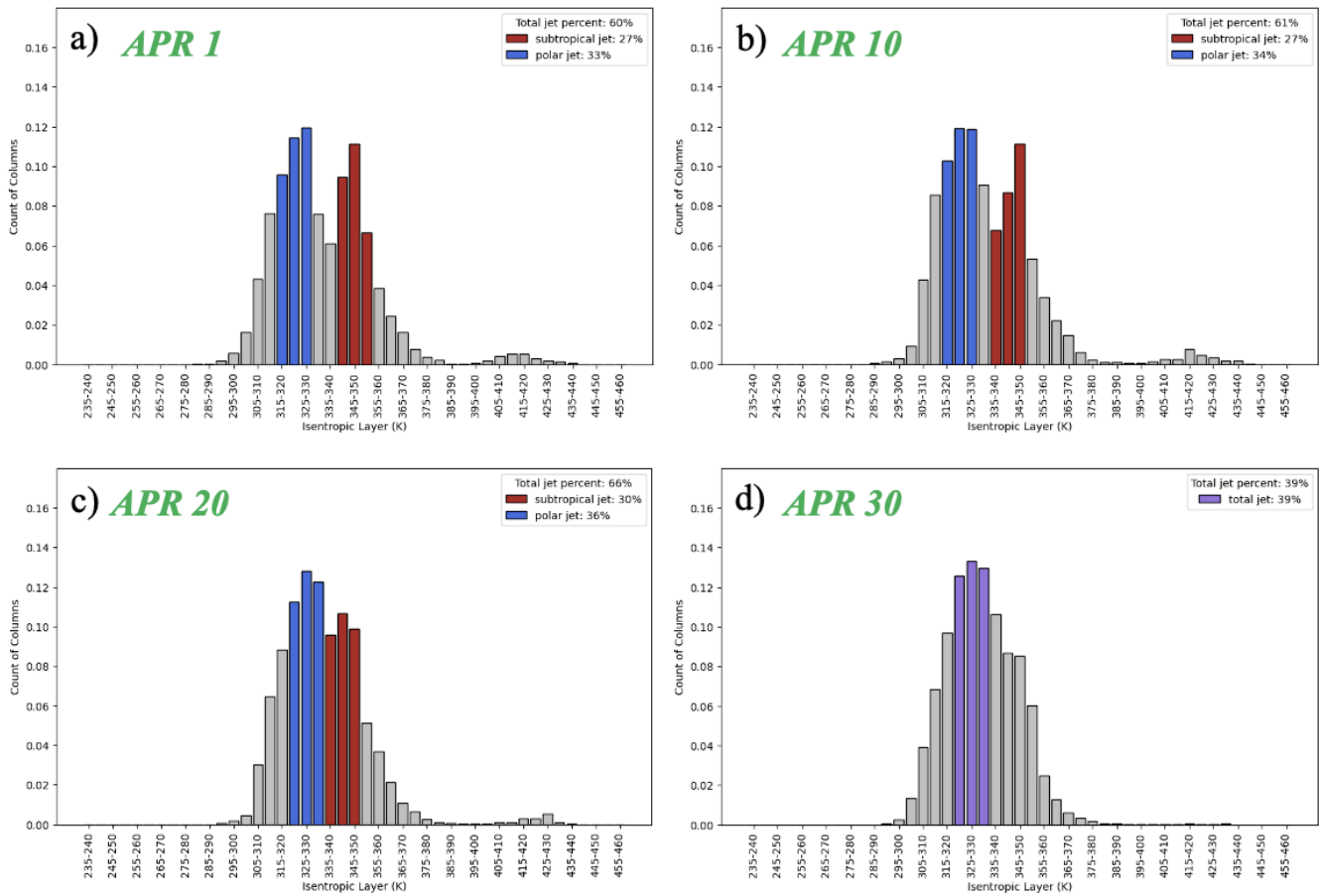


Figure 3.2: The NCEP portrayal of the jet stream distribution transition from bimodality to unimodality in the month of April, signaling the start of the warm season (May - October). The y-axis is presented at a smaller scale than in prior histogram figures to better depict the modality transition.

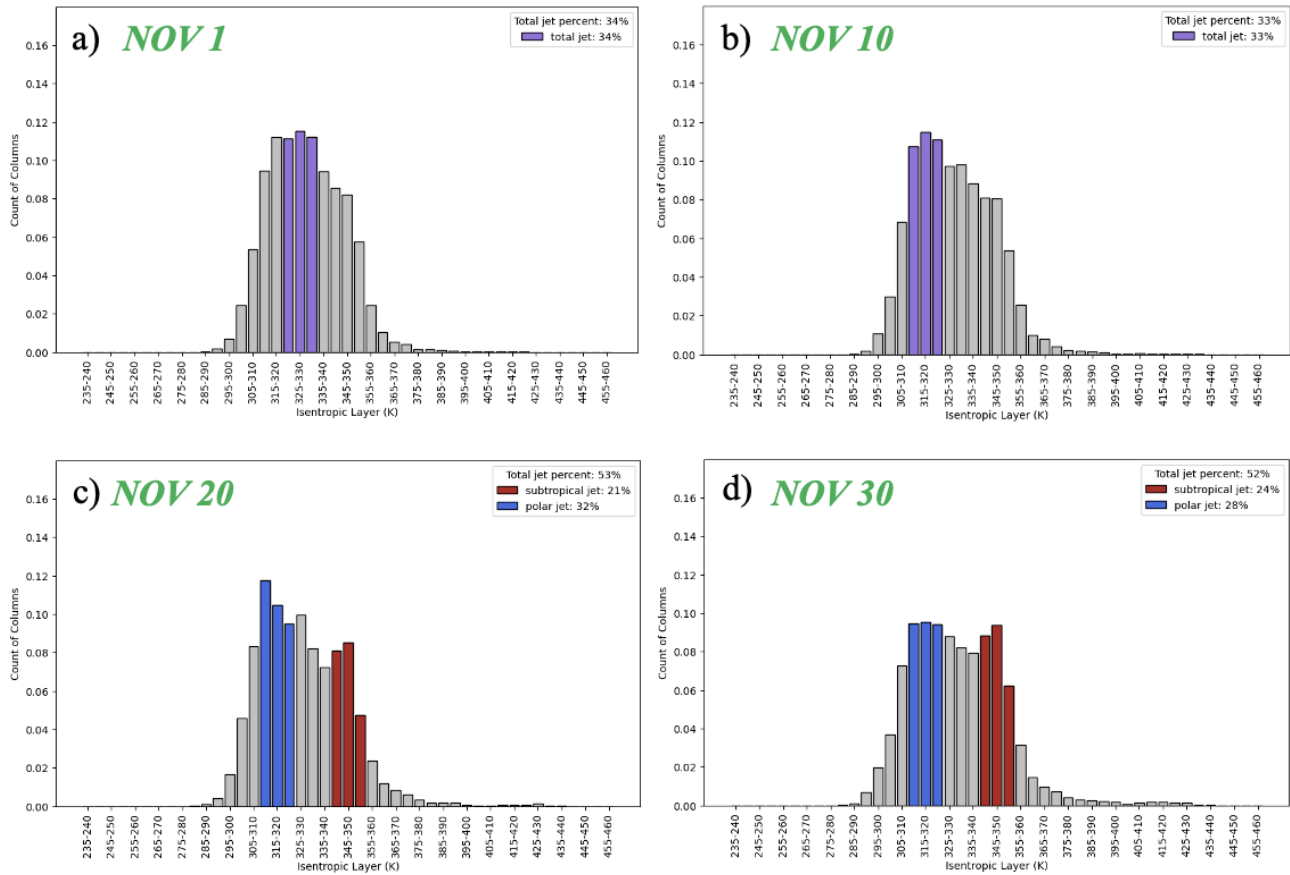


Figure 3.3: The NCEP portrayal of the jet stream distribution transition from unimodality back to bimodality in the month of November, signaling the start of the cold season (Dec. – Mar.). The y-axis is presented at a smaller scale than in prior histogram figures to better depict the modality transition.

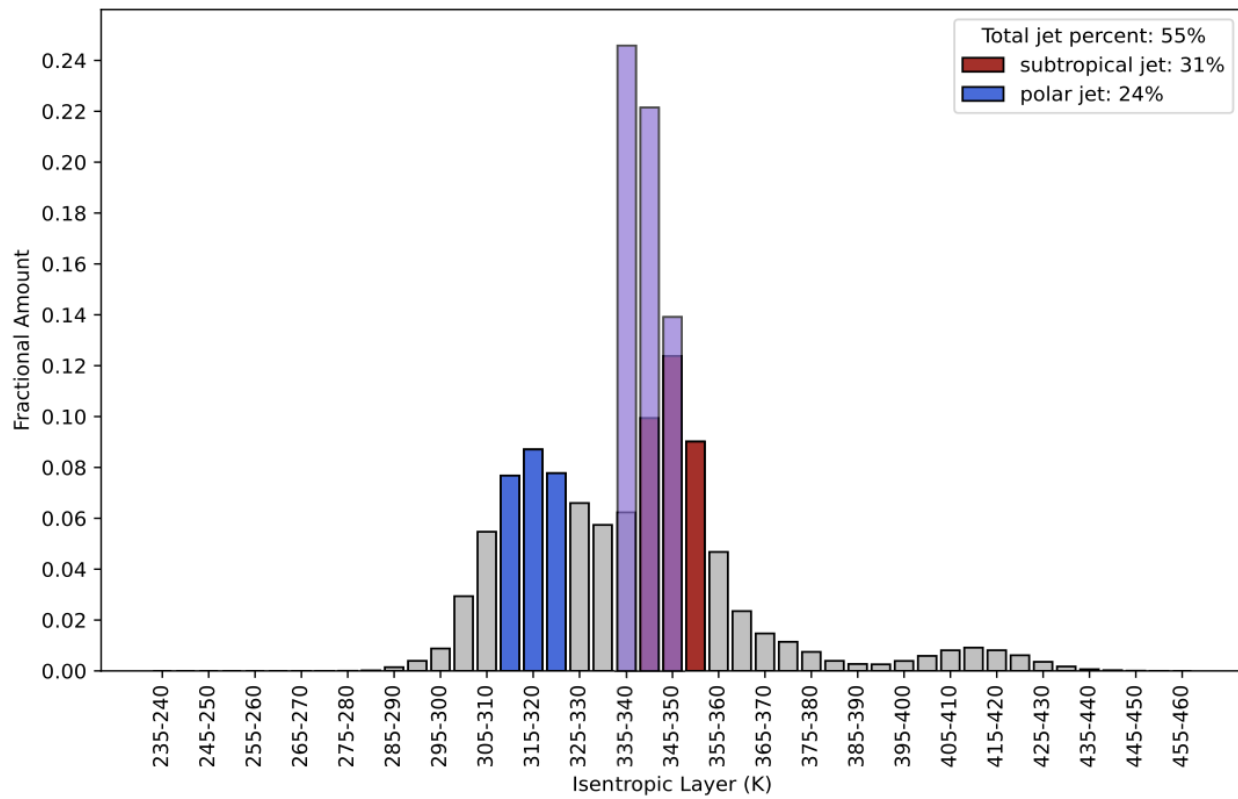


Figure 3.4: An overlay of the jet distributions for the months of January and July as seen in the NCEP dataset. The warm season unimodal jet (purple) overlaps a portion of the cold season subtropical jet (red) in isentropic space.

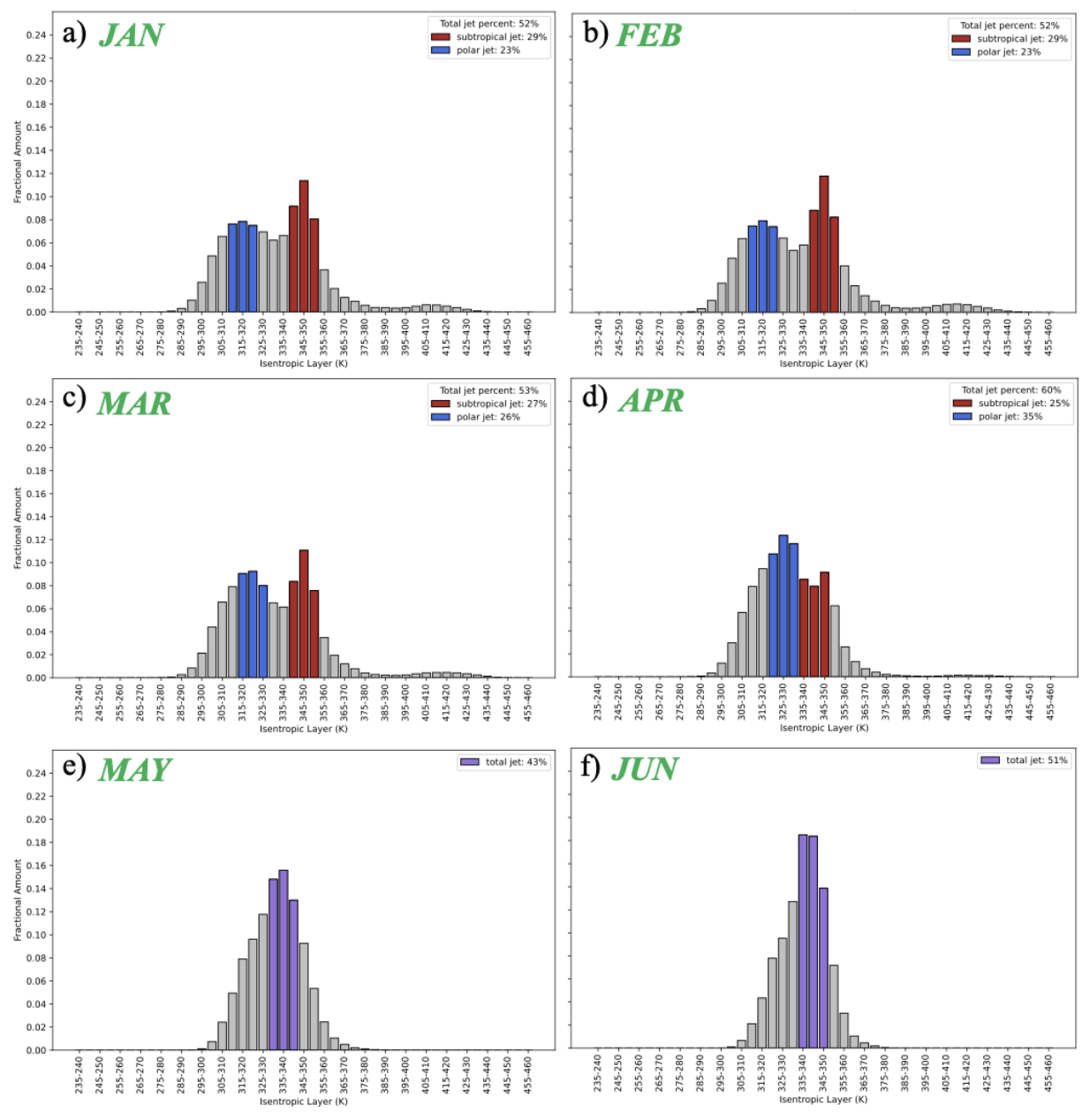


Figure 3.5: A calendar-year climatology of the Northern Hemisphere jet distribution as depicted by the ERA5 dataset. The polar and subtropical jets are represented by blue and red columns, respectively, while the single warm season jet is denoted in purple (Jan. - Jun.).

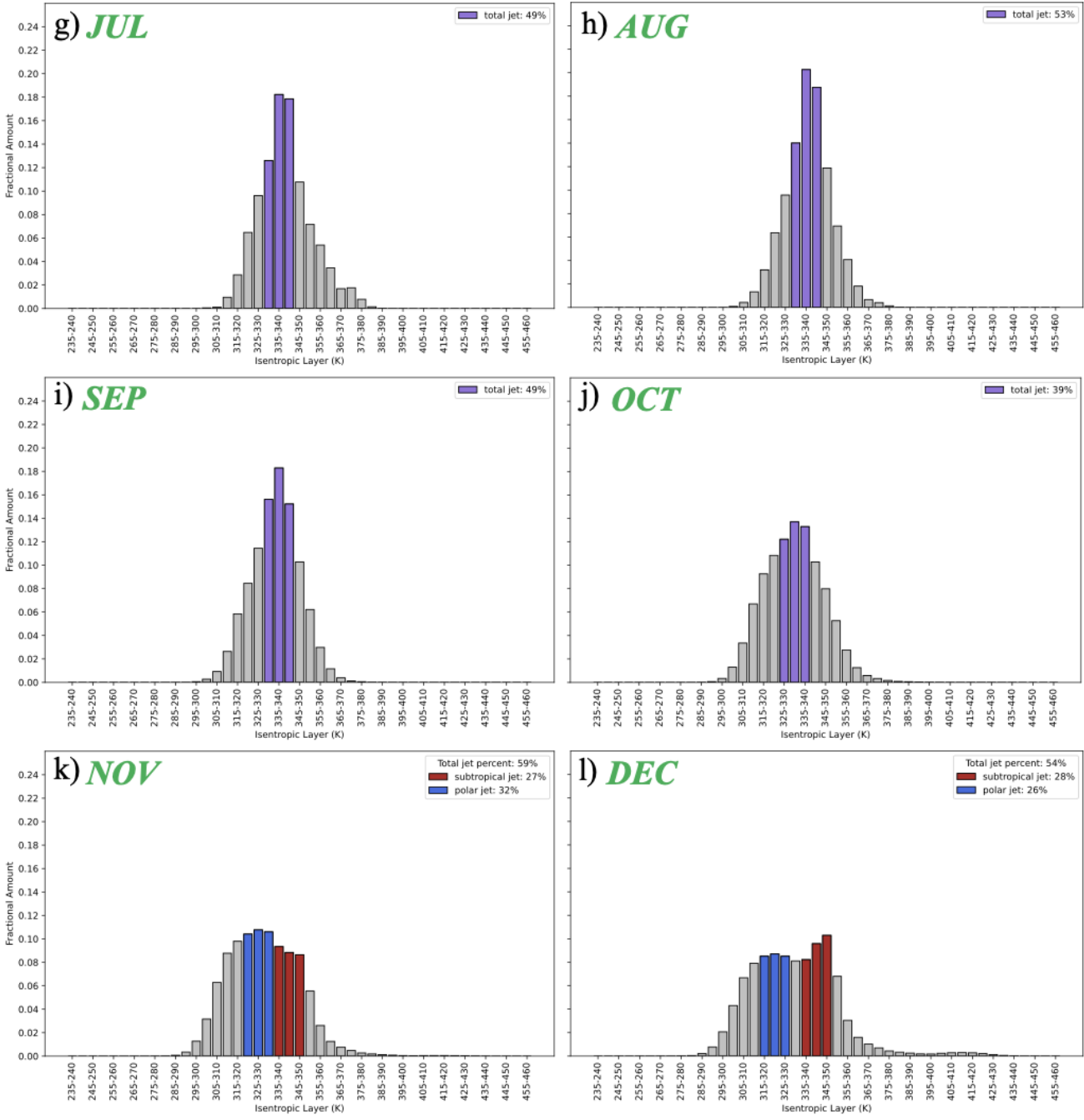


Figure 3.5 (continued): (Jul. – Dec.)

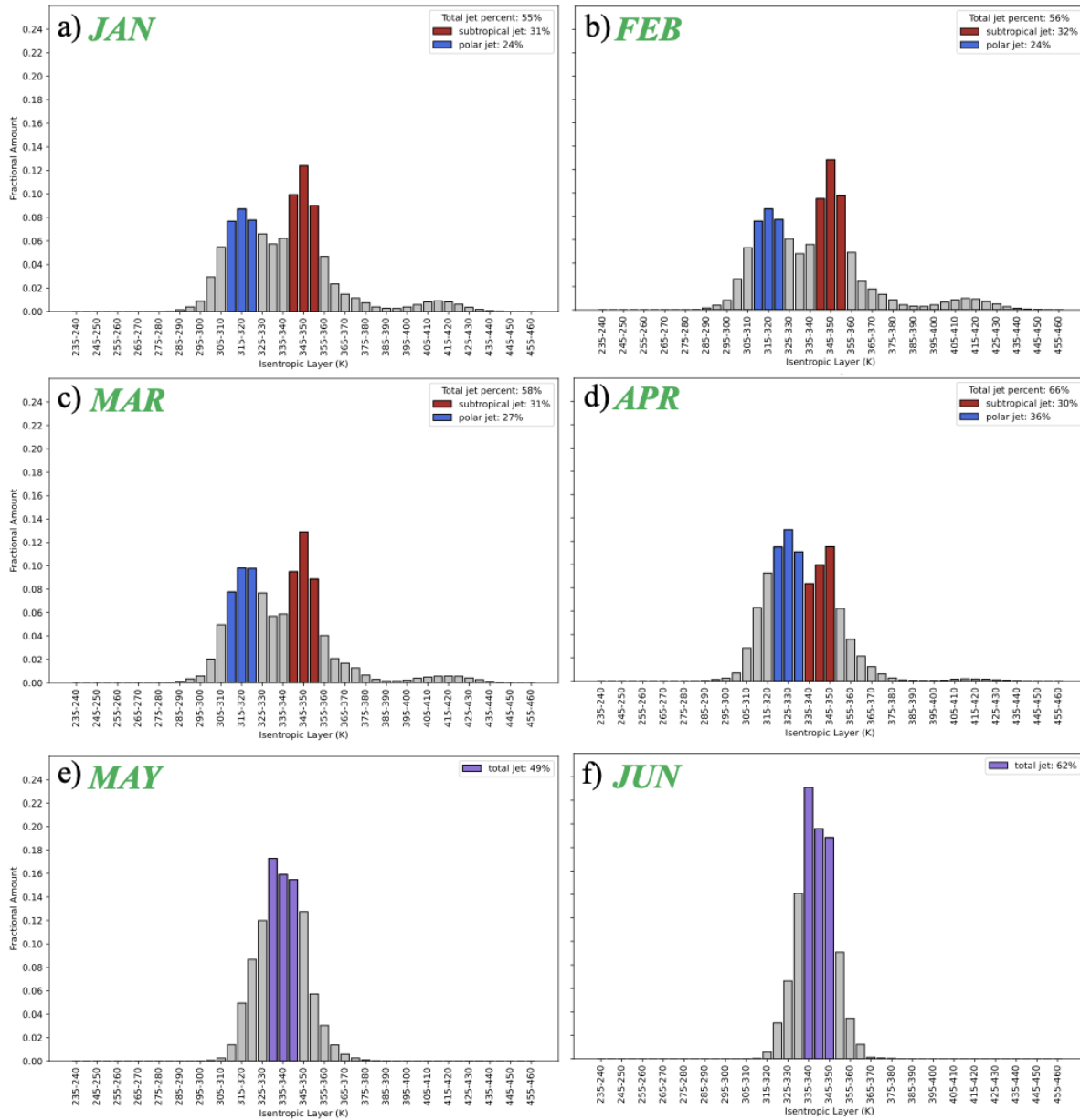


Figure 3.6: A calendar-year climatology of the Northern Hemisphere jet distribution as depicted by the NCEP dataset. The polar and subtropical jets are represented by blue and red columns, respectively, while the single warm season jet is denoted in purple (Jan. – Jun.).

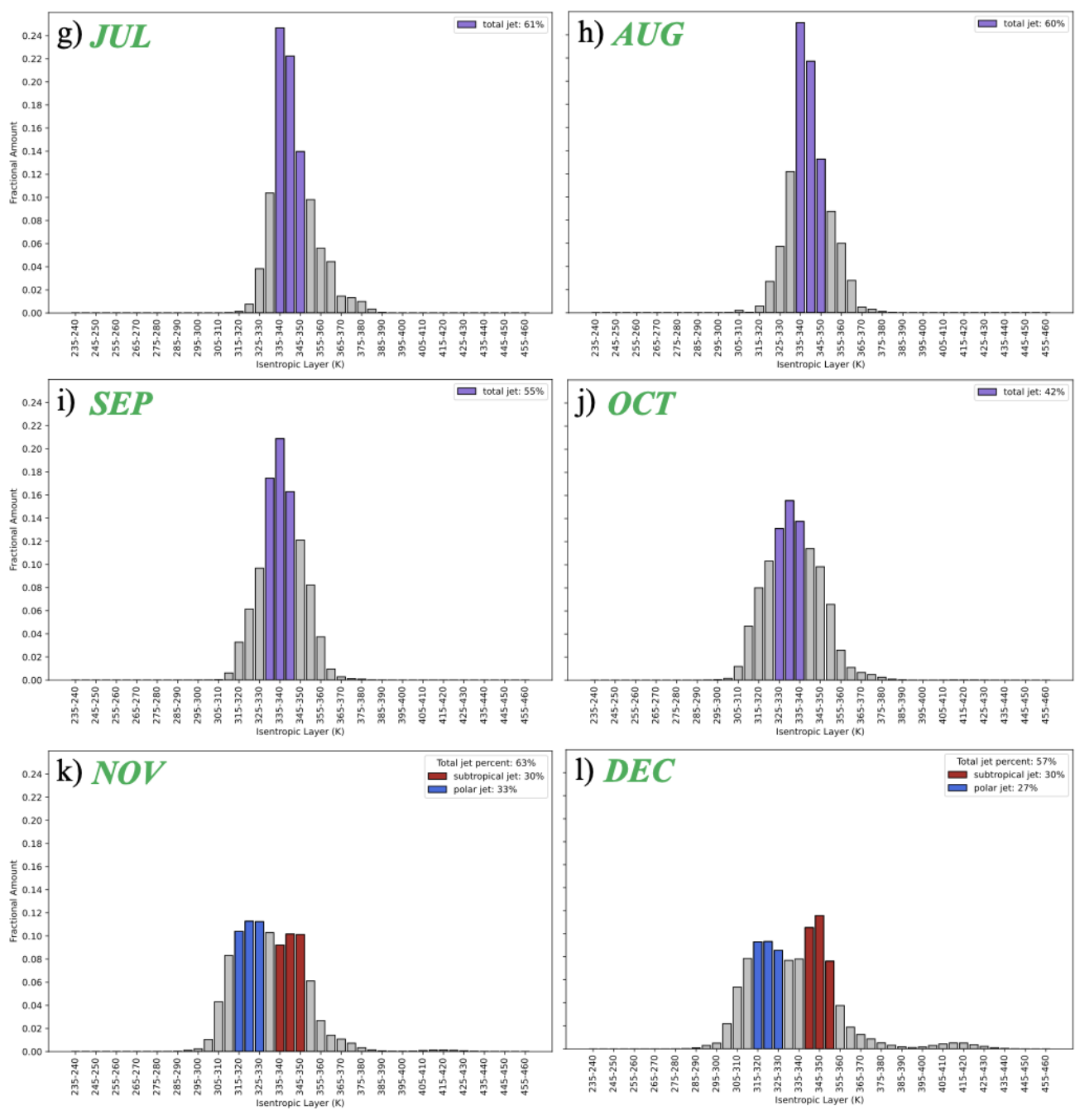


Figure 3.6 (continued): (Jul. – Dec.)

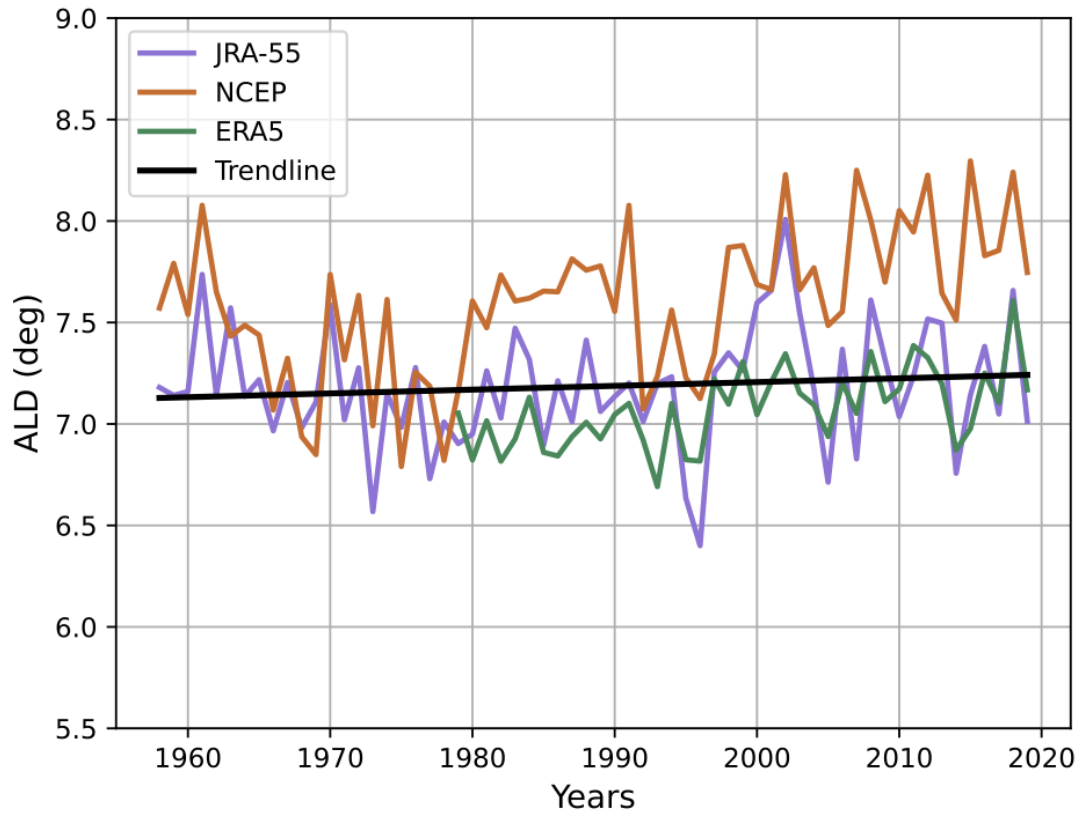


Figure 3.7: Seasonal average ALD (in degrees) of the unimodal warm season jet (May - October). Each of the colors represents a different reanalysis time series. The straight black line through each time series represents the trend line (taken from the JRA-55 data) for each. The trend line exhibits a significant trend for the ERA5 and NCEP datasets.

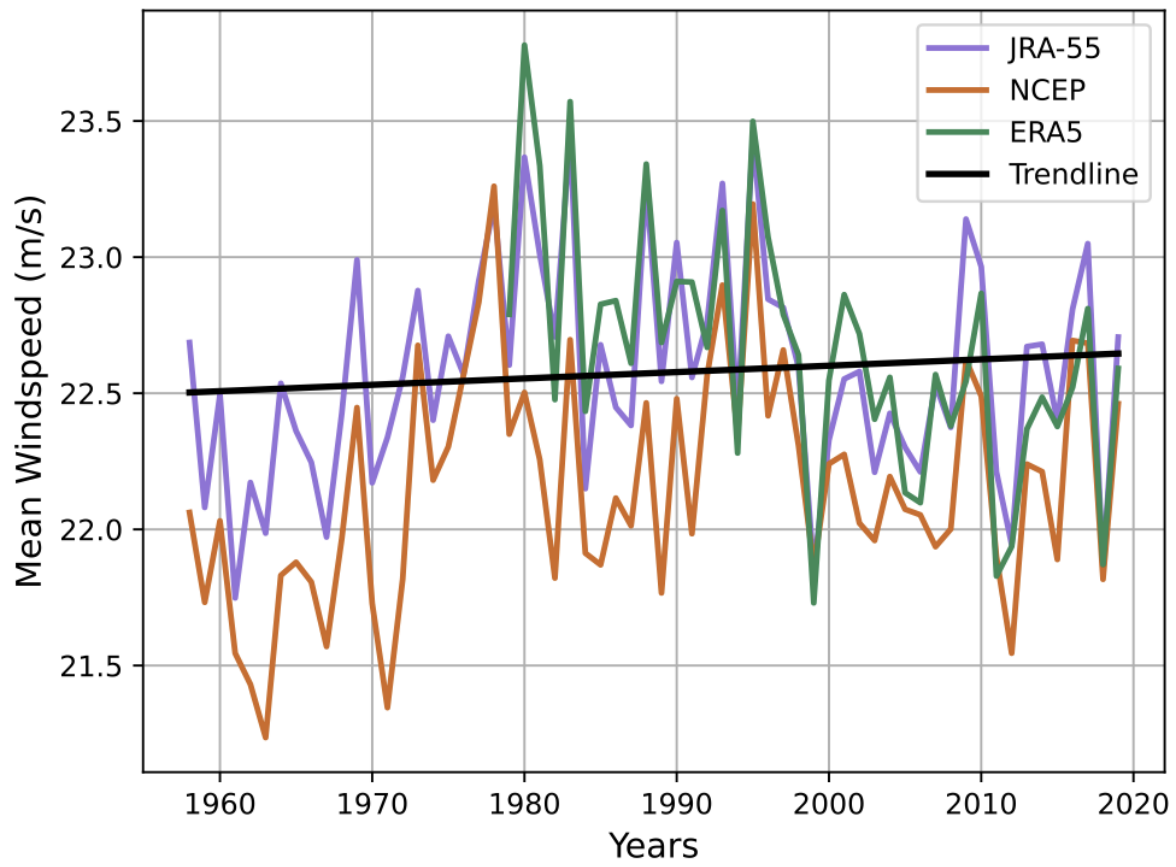


Figure 3.8: Average wind speed (m s^{-1}) along the core isertel of the warm season (May - October) unimodal jet. Each of the colors represents a different reanalysis time series. The straight black line represents the trend line for the JRA-55 dataset. Over the time series, ERA5 exhibits a significant decrease in wind speeds whereas NCEP displays a significant increase in wind speeds.

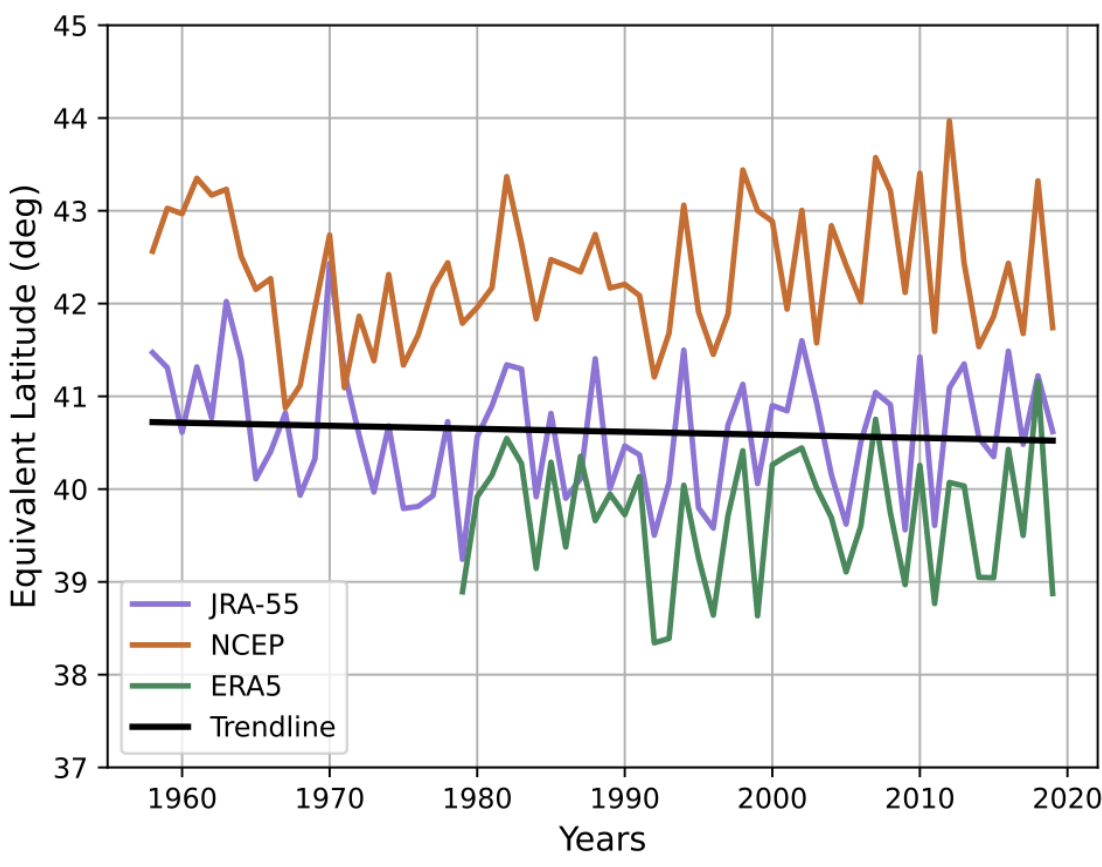


Figure 3.9: Seasonal average equivalent latitude of the unimodal warm season (May - October) jet. Each of the colors represents a different reanalysis time series. The straight black line through each time series represents the trend line (taken from the JRA-55 data) for each. The trend line does not exhibit a significant trend for any dataset.

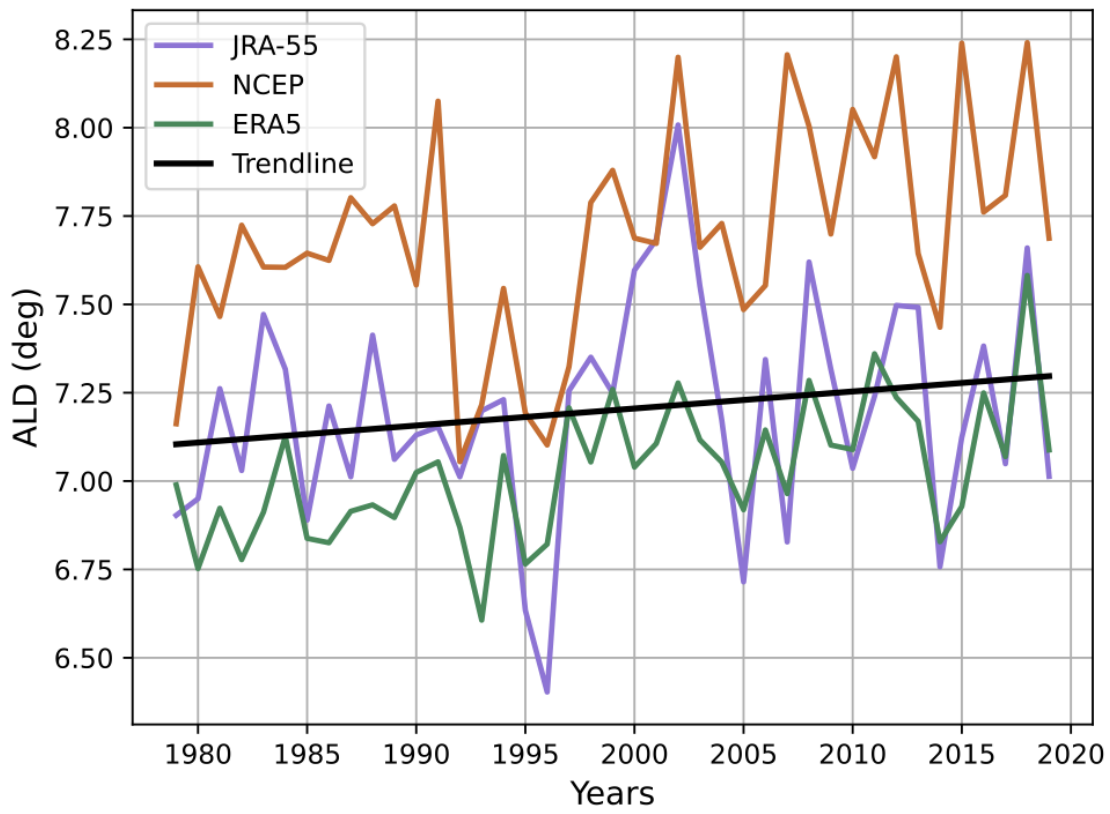


Figure 3.10: Seasonal average ALD of the warm season (May - October) unimodal jet confined to the satellite era (1979 - 2019). Each of the colors represents a different reanalysis time series. The straight black line through each time series represents the trend line (taken from the JRA-55 data) for each. ALD is increasing at a significant rate in the ERA5 and NCEP data sets only.

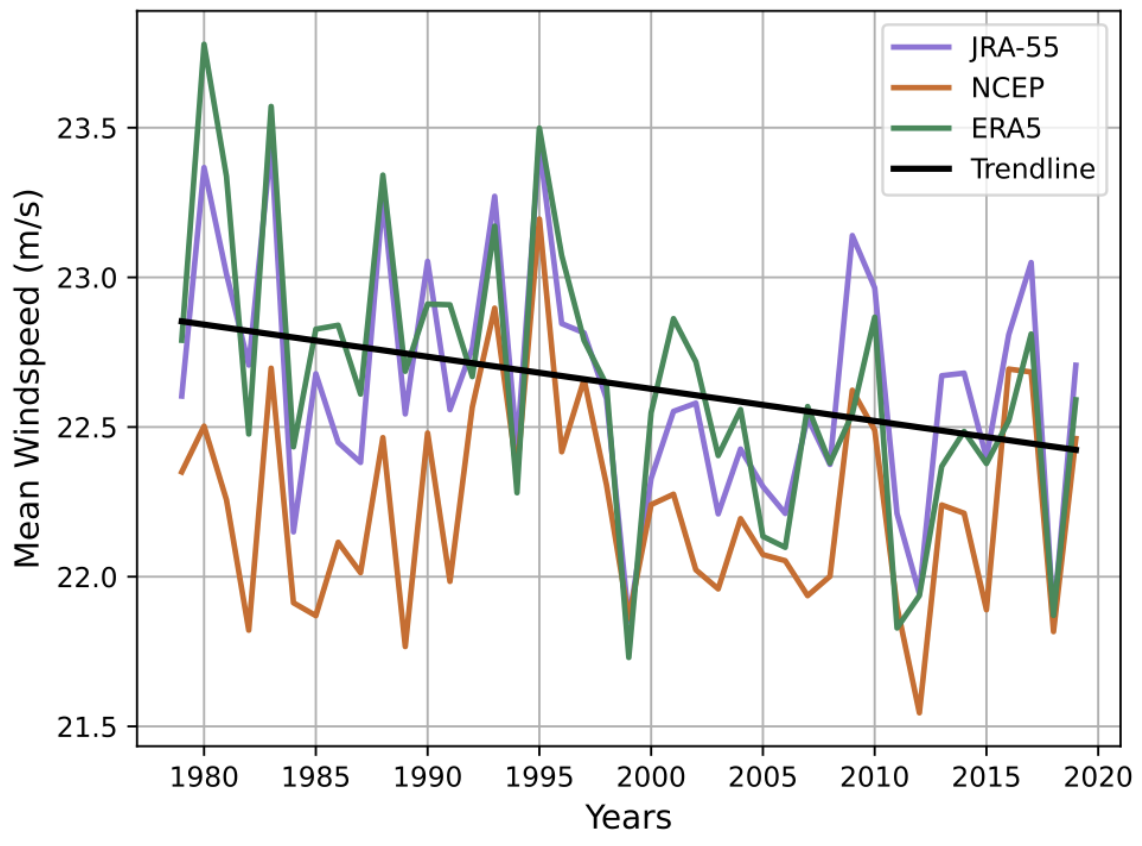


Figure 3.11: Average wind speed (m s^{-1}) of the warm season (May - October) unimodal jet core confined to the satellite era (1979 - 2019). Each of the colors represents a different reanalysis time series. The straight black line through each time series represents the trend line (taken from the JRA-55 data) for each. Wind speeds are significantly decreasing in the JRA-55 and ERA5 data sets while NCEP data exhibits no significant trend.

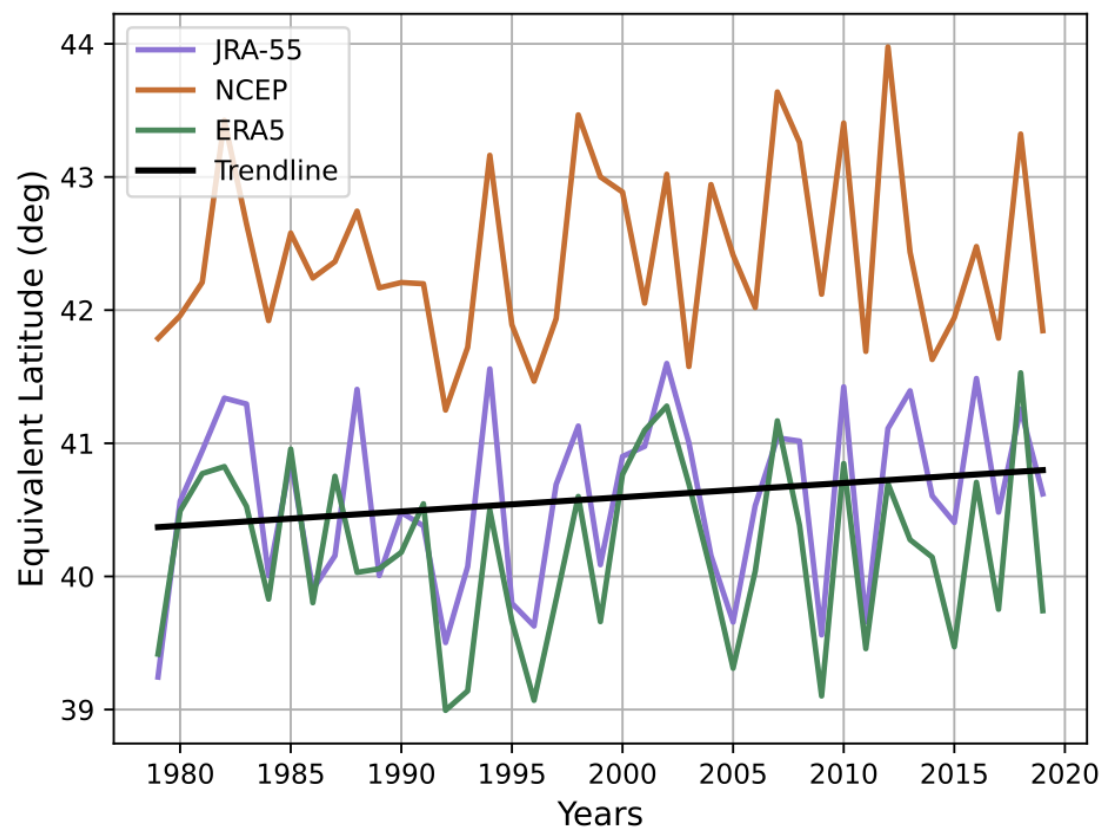


Figure 3.12: Average equivalent latitude of the warm season (May - October) unimodal jet confined to the satellite era (1979 - 2019). Each of the colors represents a different reanalysis time series. The straight black line through each time series represents the trend line (taken from the JRA-55 data) for each. All three data sets exhibit relatively weak slopes and have no significant trends.

Month	NCEP		JRA		ERA	
	Polar	Subtropical	Polar	Subtropical	Polar	Subtropical
1	310-325	340-355	310-325	340-355	310-325	340-355
2	310-325	340-355	310-325	340-355	310-325	340-355
3	310-325	340-355	310-325	340-355	315-330	340-355
4	320-335	335-350	320-335	335-350	320-335	335-350
5	330-345		330-345		330-345	
6	335-350		335-350		335-350	
7	335-350		330-345		330-345	
8	335-350		330-345		330-345	
9	330-345		330-345		330-345	
10	325-340		325-340		325-340	
11	315-330	335-350	315-330	335-350	320-335	335-350
12	315-330	340-355	310-325	335-350	315-330	335-350

Table 3.1: Isentropic housings of the polar, subtropical, and unimodal jet streams over the course of a calendar year for all three reanalysis datasets. Layers highlighted in red indicate those which are not the same across all datasets. Only 6 of 54 layers do not match, meaning 88% of all selected layers are identical.

Chapter 4

Summary & Discussion

Jet streams or jets are defined as narrow, fast-moving currents of air located near the tropopause. These features play a key role in the development of sensible weather in the mid-latitudes. In the Northern Hemisphere cold season, two main species of tropopause-level jets have been identified previously: the polar jet and the subtropical jet. The jets are separated both vertically and latitudinally and, while variable in location and intensity seasonally, have generally been assumed to be present throughout the full calendar year.

These two jets and their various characteristics have been heavily studied over time. One of the leading topics of such research in recent years has been the question of how the jets will change in a warming climate. In this thesis, three different modern reanalysis data sets (JRA-55, NCEP, and ERA5) were used to examine the isentropic location of the warm season tropopause-level jets and their trends in waviness, speed, and latitudinal location. JRA-55 and NCEP time series were truncated to cover a full 61-year time span (1959 - 2019) whereas ERA5 data covers a span of 41 years (1979 - 2019). JRA-55 and NCEP are later trimmed down to a 41-year

climatology (1979 - 2019) for an analysis over the interval corresponding to the satellite era as well, where reanalyses are expected to be more reliable.

The influential study of Koch et al. (2006) first utilized an integrated wind speed threshold to identify jet streams, which allowed for the examination of jet stream distributions in the Northern Hemisphere. The work of Christenson et al. (2017), which also considered the relationship between horizontal PV gradients and wind speed as suggested by Cunningham and Keyser (2004), further built upon this idea by taking into account both this integrated wind speed threshold as well as a PV gradient threshold within selected isentropic layers. Doing so allowed for identifying the isentropic housing for each species of jet stream by identifying peaks in the isentropic distribution of maximum wind speed. Following this methodology, their study found that during the Northern Hemisphere cold season, the polar jet resides in the 315 - 330 K layer while the subtropical jet resides in the 340 - 355 K layer. The analysis presented here follows this same methodology and recreates these results in the cold season while uniquely establishing the jet stream distribution in the Northern Hemisphere warm season. A prominent result of this analysis is the fact that in all three of the reanalysis data sets assessed, the warm season is dominated by a unimodal jet stream distribution, indicative of the presence of only one jet stream in this time frame (Figures 3.1, 3.5, 3.6). Over a full calendar year, only six isentropic layers differ across data sets (as seen in Table 3.1). This single warm season jet resides in the 330 - 345 K isentropic layer (somewhat of a middle ground between the two isentropic housings found in the cold season) and is a characteristic evident in all three data sets, though it does exhibit some minor variations in the first and last months of the warm season. Furthermore, the months of April and November serve as transitional periods in which the jet distribution switches from bimodal to unimodal and from unimodal back to bimodal, respectively (Figures 3.2, 3.3).

Once the isentropic housing of a jet is established, assessment of its waviness and several other characteristics can be made employing the average latitudinal displacement methodology (ALD) developed by Martin (2021). In this methodology, a “core isertel”, along which the hemispheric circulation per unit length is maximized, is found for the jet. This core isertel acts as a proxy for the axis of a jet core. The area enclosed by the core isertel is equated to that poleward of a zonal ring referred to as its equivalent latitude, which is a close proxy for the zonally averaged latitude of the jet core on a given day. Summing the latitudinal departures of the core isertel from its equivalent latitude (at each longitude in the data) yields the average latitudinal displacement (ALD) of the jet which serves as a measure of waviness. Along with the equivalent latitude and the average jet core speed (i.e. the average speed along the core isertel), several salient characteristics of the jet are assessed. Martin (2021) originally applied this methodology over the same three datasets to the Northern Hemisphere cold season (DJF). During this period, both the polar and subtropical jets are distinctly present, meaning trends in several characteristics are available for assessment.

When comparing the findings of Martin (2021) to those presented here over the full 61-year period, trends are found to sometimes differ between seasons. For both the polar and subtropical jets in the cold season, no significant trends in average speed were present in any of the three data sets. In the full warm season climatology, however, each data set displays a different speed trend over time. Over this time period ERA5 exhibits a significant decrease in jet wind speeds whereas NCEP displays a significant increase. JRA-55 shows no significant trend in wind speed, further contributing to the poor agreement across data sets in the warm season. When these trends are considered in a truncated 41-year climatology, however, both JRA-55 and

ERA5 portray a jet that has significantly slowed with time while NCEP depicts no significant trends whatsoever.

The cold season was also characterized by a poleward encroachment of both jets, the polar jet doing so at a faster rate than the subtropical jet. In the warm season, however, there is no movement of the unimodal jet poleward or equatorward in any data set for both the 41- and 61-year time climatology. The unimodal jet has remained in the same general location, neither moving poleward or equatorward. Overall, the greatest agreement between the two analyses is in the assessment of jet waviness. During the cold season, both jets are becoming systematically wavier over time. In both time frames of the warm season, the ERA5 and NCEP data sets depict the unimodal jet becoming wavier with time, albeit at a modest rate. Ultimately, trends of this unimodal jet are somewhat variable across data sets and generally differ from those of the polar and subtropical jets in the cold season.

The NCEP data set's results tend to be outliers in all portions of this analysis. When examining the isentropic distribution and location of the jet in the warm season (as seen in Section 3.1) NCEP data contained the most discrepancies when compared to the other data sets. Table 3.1 depicts the isentropic housings of the Northern Hemisphere jet streams over a full calendar year for each data set. Across all housings, only six layers differ. Three of these different housings belong to the NCEP data set. These discrepancies also arose when examining the trends in jet wind speed, latitudinal location, and waviness over both 61-year and 40-year time series (Figures 3.7, 3.8, 3.9, 3.10, 3.11, 3.12). Compared to the other data sets, NCEP frequently was notably higher or lower than those seen with ERA5 or JRA-55. Trendline slopes for NCEP also were usually much more drastic than the other datasets and occasionally even portrayed slopes of opposite value than the others. Other analyses (e.g. Xu et al. 2021) have also

encountered similar disparities when comparing data sets, which they attributed in part to lack of detail in NCEP data. The ERA5 data set has improved representation of convective updrafts, gravity waves and other meso- to synoptic-scale features that can enhance mixing whereas NCEP and JRA-55 have lower resolutions that can diminish this mixing. These core differences in the spatial and temporal resolutions of the datasets likely underlie the discrepancies seen within this study.

Numerous other studies have attempted to evaluate various jet characteristics and respective trends with their own unique methods over a variety of time frames (e.g., Strong and Davis 2007; Archer and Caldeira 2008; Manney and Hegglin 2018; Martin 2021). Some offer warm season trends that can be compared to the findings in the present analysis. Archer and Caldeira (2008) used mass-weighted wind speeds to assess characteristics of jet streams in both hemispheres. In their study they did not emphasize a distinct separation between the subtropical and polar jets in any season in the Northern Hemisphere. They did, however, see the Northern Hemisphere summertime jet (in their study, JJA) exhibit a subtle poleward encroachment and an overall slight decrease in wind speed.

Manney and Hegglin (2018) employed wind speed maxima and jet latitudinal location to characterize trends of a two jet structure over a full calendar year for both hemispheres. They found that in the Northern Hemisphere summer (in their study, JJA) the polar jet sees a decrease in speeds over the North American and Atlantic regions and tends to move equatorward in all seasons. Conversely, the subtropical jet saw no distinct latitudinal shifts in the summer but did see a significant wind speed decrease over the western Pacific. Recall that within the present study, a unimodal jet was found to exist in the Northern Hemisphere warm season. This unimodal jet had no significant changes in latitude and, while variable in the full climatology,

portrayed a slowing jet stream in the JRA-55 and ERA5 41-year climatology. Despite examining a two jet structure, the Manney and Hegglin (2018) findings do somewhat align with those within the present analysis. Even with these varying methodologies and time frames, their broad jet stream warm season trends tend to align with those seen within the present analysis.

The similarities in results between the Manney and Hegglin (2018) study and the present analysis are striking when it is considered that their results derived from analysis of a two jet structure in the warm season whereas the present study featured a unimodal jet structure. Therefore, it is worth taking a deeper dive into the similarities and differences in the methodologies of both analyses. Manney and Hegglin (2018) utilized a methodology that built upon what was developed in Manney et al. (2011, 2014, 2017). These studies identified tropopause-level jets wherever a wind speed maximum greater than 40 ms^{-1} was located. The boundaries of these jets were defined as the points surrounding the jet maxima which fall below 30 ms^{-1} , a criterion based on that seen in Koch et al. (2006). In addition to this wind speed criteria, these studies differentiated between the polar and subtropical jets based on their latitudinal placements. In their more recent analysis (Manney and Hegglin 2018), they define the subtropical jet as the most equatorward westerly jet for which the tropopause altitude at the jet's equatorward edge is greater than 13.0 km. This jet must also feature a drop in tropopause altitude from its equatorward side to its poleward side of at least 2.0 km. Once the subtropical jet is established, they define the polar jet as the strongest westerly jet poleward of the subtropical jet. If no subtropical jet is found, the strongest westerly jet poleward of 40° becomes the polar jet. This ultimately separates the jets into the subtropical jet, which is identified by a break in the tropopause, and the polar jet, which is identified as the primarily eddy driven jet. This is likely where the discrepancies between their study and the research presented here arise.

The Manney method of identification of tropopause-level jets relies, to a fair degree, on their latitudinal location. As a consequence of this method, there will always be at least a polar jet identified. The research presented within this thesis identifies jets only where the Koch et al. (2006) wind speed criteria is met and places these jets into their respective isentropic housings. This allows for the construction of an isentropic distribution of the level of maximum wind, which in turn reveals the location of jet streams in isentropic space for each month of the year. Results of this analysis depict a bimodal jet structure, a unimodal jet structure, and even a glimpse of the polar night jet (as can be seen in the 400 - 430 K range in Figures 3.1a and 3.1b) dependent on which season is examined. Ultimately, the differing methodologies between the present study and Manney and Hegglin (2018) have little overlap as they rely on tropopause height and latitudinal specifications whereas the present study depends on integrated wind speed and location in isentropic space. The methodology used here also does not default to there always being a polar jet present, which is a caveat that likely results in these differences in warm season jet structure.

The concept of the Northern Hemisphere containing only one dominant jet stream throughout its warm season provides plenty of opportunity for additional future work. As of now the origins of this unimodal jet remain unclear. Whether it is a result of the polar or subtropical jet becoming more dominant or rather a combination of the two remains to be explored in the future. Similarly, it is well established that jet streams reside in the same locations as tropopause steps. As such, one may expect there to be a single slightly larger tropopause step in the warm season as there is only one distinct jet structure.

While it is presented here hemispherically, this methodology can also be broken down to assess smaller, more regional areas. Regional analyses of characteristics such as jet waviness or

wind speed may lead to the discovery of more significant and notable trends, allowing for the identification of which regions contribute most to the overall hemispheric trends. Jet streams are also tied to smaller scale convective weather systems and their development during the warm season. Various jet characteristics such as speed, waviness, and location often have an impact on the severity and location of these storms. Being able to fully characterize the relationship between a changing warm season jet and its potential impacts on these convective systems would prove useful to both the research and operational fields of atmospheric science. Finally, the distribution of warm season tropopause-level jet streams and their various characteristics can also be examined in the Southern Hemisphere.

Considering this jet in the case of a warming climate also allows for the development of several other research questions, some of which can be evaluated here. Have April and November contained the jet modality transitions throughout the entire analysis period, or did these transitions arrive earlier/later as winters become warmer and summers become longer? A quick assessment of this question reveals that the transitions have undergone little change in the examined time period. An example of this is provided in Figures 4.1 and 4.2, which depict November's unimodal to bimodal transition in the first half of the JRA-55 data set (1959-1988) and the second half of the data set (1989-2019), respectively. The modality transition is still present in both time periods. November 1st and 10th are very similar in both figures, both showing the unimodal jet that is still remnant from the warm season. The earlier time period, however, depicted the unimodal jet at a slightly lower isentropic level than the later time period. In other words, this means the unimodal jet has shifted to a slightly warmer isentropic level over time in the first half of November. A bimodal pattern is seen on November 20th and 30th in both figures as well. Both of the time periods have very similar distributions, with each jet appearing

to reside in the same isentropic housings in both figures. Any indication of the jet modality transitions changing due to warming global temperatures is seen only in the early portions of November.

When this examination was applied to April there were also no visible changes between time periods (not shown). More detailed analysis of this question, however, may provide further insight into the transitions. Another similar question is that, since a unimodal jet structure dominates the warm season, could it persist into other seasons if warmer average temperatures exist year round? Assessing either of these questions using data from a climate model would offer further insight into projected jet stream distributions and patterns as well as providing trends which may not be inferred from present reanalysis data.

Tropopause-level jet streams are some of the most ubiquitous features in Earth's atmosphere. These structures have direct ties to both synoptic-scale weather systems and circulations on a global scale. Analyzing their evolutions and trends over the course of a calendar year (as is the research focus of this thesis) allows for the better understanding of these systems both in the present and future climates.

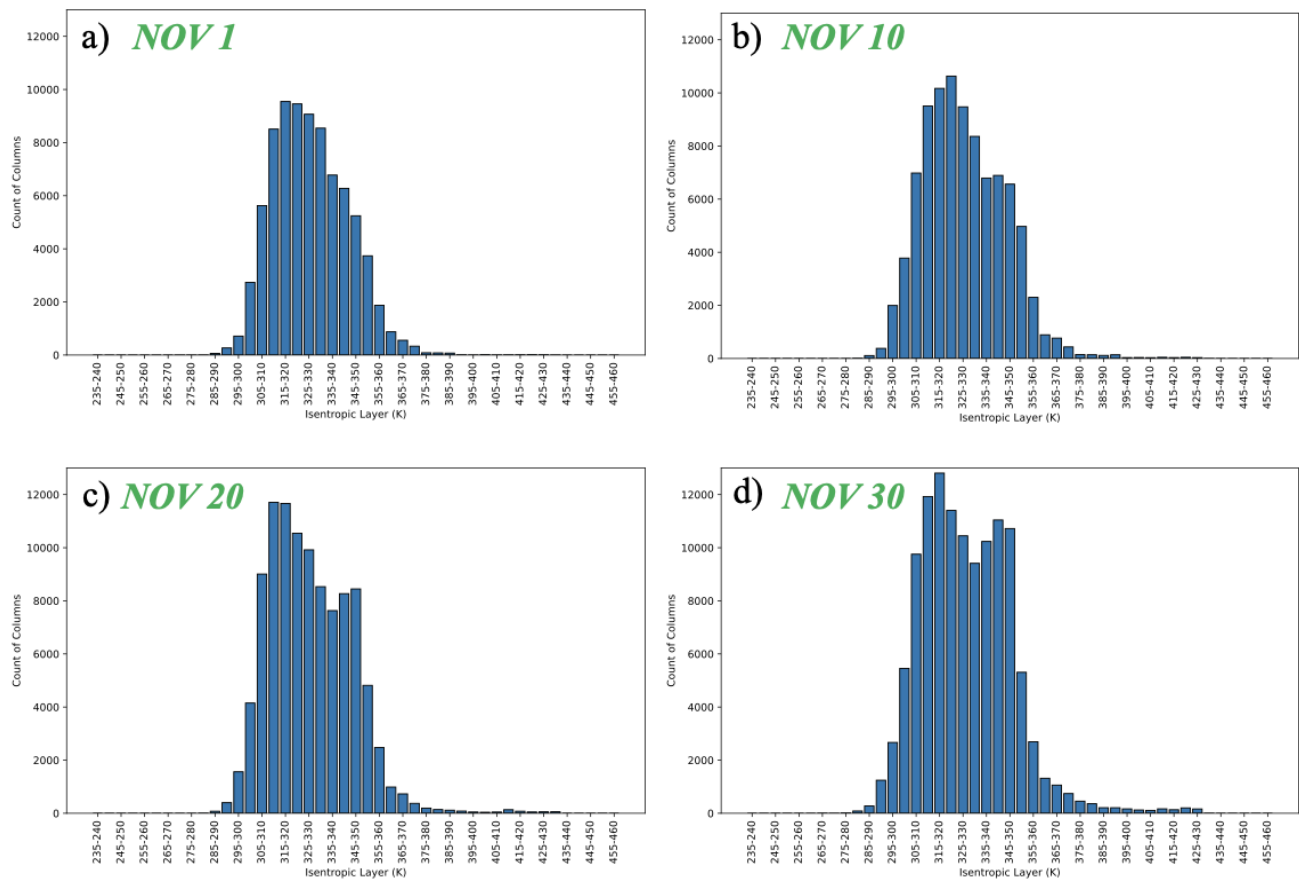


Figure 4.1: The JRA-55 data set’s depiction of the unimodal to bimodal jet distribution transition in the month of November for the years 1959 – 1988. The lower overall count of columns is an artifact of shortening the examined timescale.

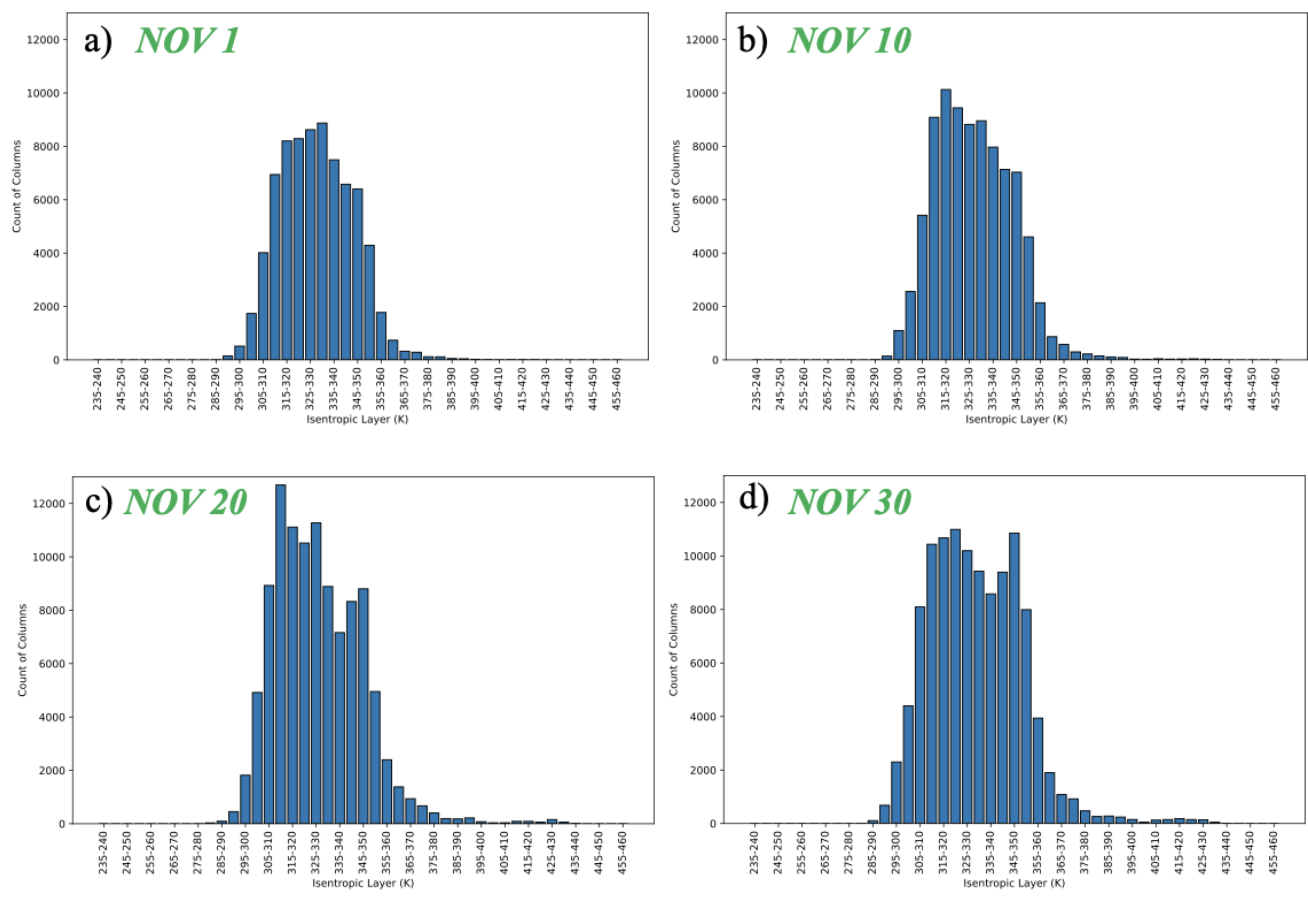


Figure 4.2: The JRA-55 data set’s depiction of the unimodal to bimodal jet distribution transition in the month of November for the years 1989 – 2019 . The lower overall count of columns is an artifact of shortening the examined timescale.

Bibliography

- Archer, C. L., and K. Caldeira, 2008: Historical trends in the jet streams. *Geophysical Research Letters*, **35**, <https://doi.org/10.1029/2008GL033614>.
- Athanasiadis, P. J., J. M. Wallace, and J. J. Wettstein, 2010: Patterns of Wintertime Jet Stream Variability and Their Relation to the Storm Tracks. <https://doi.org/10.1175/2009JAS3270.1>.
- Barnes, E. A., 2013: Revisiting the evidence linking Arctic amplification to extreme weather in midlatitudes. *Geophysical Research Letters*, **40**, 4734–4739, <https://doi.org/10.1002/grl.50880>.
- , and L. Polvani, 2013: Response of the Midlatitude Jets, and of Their Variability, to Increased Greenhouse Gases in the CMIP5 Models. <https://doi.org/10.1175/JCLI-D-12-00536.1>.
- Barnes, E. A., and J. A. Screen, 2015: The impact of Arctic warming on the midlatitude jet-stream: Can it? Has it? Will it? *WIREs Climate Change*, **6**, 277–286, <https://doi.org/10.1002/wcc.337>.
- Bell, B., and Coauthors, 2020: Satellite observations in support of the Copernicus Climate Change Service. *Space, Satellites, and Sustainability*, Vol. 11527 of, Space, Satellites, and Sustainability, SPIE, 23–32. <https://doi.org/10.1117/12.2576497>
- Blackport, R., and J. A. Screen, Insignificant effect of Arctic amplification on the amplitude of midlatitude atmospheric waves. <https://doi.org/10.1126/sciadv.aay2880>.
- Bretherton, F. P., 1966: Critical layer instability in baroclinic flows. *Quarterly Journal of the Royal Meteorological Society*, **92**, 325–334, <https://doi.org/10.1002/qj.49709239302>.
- Burt, M. A., D. A. Randall, and M. D. Branson, 2016: Dark Warming. *J. Climate*, **29**, 705–719, <https://doi.org/10.1175/JCLI-D-15-0147.1>.

- Chen, G., J. Lu, D. A. Burrows, and L. R. Leung, 2015: Local finite-amplitude wave activity as an objective diagnostic of midlatitude extreme weather. *Geophysical Research Letters*, **42**, 10,952–10,960, <https://doi.org/10.1002/2015GL066959>.
- Christenson, C. E., J. E. Martin, and Z. J. Handlos, 2017: A Synoptic Climatology of Northern Hemisphere, Cold Season Polar and Subtropical Jet Superposition Events. <https://doi.org/10.1175/JCLI-D-16-0565.1>.
- Copernicus Climate Change Service (C3S). (2017). *ERA5: Fifth generation of ECMWF atmospheric reanalyses of the global climate*. Copernicus Climate Change Service Climate Data Store (CDS). Retrieved from <https://cds.climate.copernicus.eu/cdsapp#!/home>
- Coumou, D., V. Petoukhov, S. Rahmstorf, S. Petri, and H. J. Schellnhuber, 2014: Quasi-resonant circulation regimes and hemispheric synchronization of extreme weather in boreal summer. *Proceedings of the National Academy of Sciences*, **111**, 12331–12336, <https://doi.org/10.1073/pnas.1412797111>.
- Cunningham, P., and D. Keyser, 2004: Dynamics of jet streaks in a stratified quasi-geostrophic atmosphere: Steady-state representations. *Quarterly Journal of the Royal Meteorological Society*, **130**, 1579–1609, <https://doi.org/10.1256/qj.03.35>.
- Davies, H. C., and A. M. Rossa, 1998: PV Frontogenesis and Upper-Tropospheric Fronts. *Monthly Weather Review*, *126*, 1528–1539. [https://doi.org/10.1175/1520-0493\(1998\)126<1528:pfauf>2.0.co;2](https://doi.org/10.1175/1520-0493(1998)126<1528:pfauf>2.0.co;2)
- Davis, C. A., and K. A. Emanuel, 1991: Potential Vorticity Diagnostics of Cyclogenesis. *Monthly Weather Review*, *119*, 1929–1953. [https://doi.org/10.1175/1520-0493\(1991\)119<1929:pvdof>2.0.co;2](https://doi.org/10.1175/1520-0493(1991)119<1929:pvdof>2.0.co;2)
- Defant, F., and H. Taba, 1957: The Threefold Structure of the Atmosphere and the Characteristics of the Tropopause. *Tellus A: Dynamic Meteorology and Oceanography*, **9**, <https://doi.org/10.3402/tellusa.v9i3.9112>.

- Di Capua, G., and D. Coumou, 2016: Changes in meandering of the Northern Hemisphere circulation. *Environ. Res. Lett.*, **11**, 094028, <https://doi.org/10.1088/1748-9326/11/9/094028>.
- Ertel, H. (1942). Ein Neuer hydrodynamischer Wirbelsatz. *Meteorologische Zeitschrift*, *59*, 271–281.
- Francis, J. A., 2017: Why Are Arctic Linkages to Extreme Weather Still up in the Air? <https://doi.org/10.1175/BAMS-D-17-0006.1>.
- , and S. J. Vavrus, 2012: Evidence linking Arctic amplification to extreme weather in mid-latitudes. *Geophysical Research Letters*, **39**, <https://doi.org/10.1029/2012GL051000>.
- , and ———, 2015: Evidence for a wavier jet stream in response to rapid Arctic warming. *Environ. Res. Lett.*, **10**, 014005, <https://doi.org/10.1088/1748-9326/10/1/014005>.
- Francis, J. A., N. Skific, and S. J. Vavrus, 2018: North American Weather Regimes Are Becoming More Persistent: Is Arctic Amplification a Factor? *Geophysical Research Letters*, **45**, 11,414-11,422, <https://doi.org/10.1029/2018GL080252>.
- Grams, C. M., and Coauthors, 2011: The key role of diabatic processes in modifying the upper-tropospheric wave guide: a North Atlantic case-study. *Quarterly Journal of the Royal Meteorological Society*, **137**, 2174–2193, <https://doi.org/10.1002/qj.891>.
- Harnik, N., Garfinkel, C. I., Lachmy, O., 2016: The influence of jet stream regime on extreme weather events. *Dynamics and Predictability of Large-Scale, High-Impact, Weather and Climate Events*, Li, J., Swinbank, R., Grotjahn, R., Volkert, H., Cambridge University Press, 79-94.
- Held, I. M., 1975: Momentum Transport by Quasi-Geostrophic Eddies. *Journal of the Atmospheric Sciences*, *32*, 1494–1497. [https://doi.org/10.1175/1520-0469\(1975\)032<1494:mtbqge>2.0.co;2](https://doi.org/10.1175/1520-0469(1975)032<1494:mtbqge>2.0.co;2)

- , and A. Y. Hou, 1980: Nonlinear Axially Symmetric Circulations in a Nearly Inviscid Atmosphere. *Journal of the Atmospheric Sciences*, **37**, 515–533.
[https://doi.org/10.1175/1520-0469\(1980\)037<0515:nascia>2.0.co;2](https://doi.org/10.1175/1520-0469(1980)037<0515:nascia>2.0.co;2)
- Hoffmann, L., and Coauthors, 2019: From ERA-Interim to ERA5: the considerable impact of ECMWF's next-generation reanalysis on Lagrangian transport simulations. *Atmospheric Chemistry and Physics*, **19**, 3097–3124, <https://doi.org/10.5194/acp-19-3097-2019>.
- Hoskins, B., and P. Berrisford, 1988: A Potential Vorticity Perspective of the Storm of 15–16 October 1987. *Weather*, **43**, 122–129, <https://doi.org/10.1002/j.1477-8696.1988.tb03890.x>.
- Hoskins, B. J., M. E. McIntyre, and A. W. Robertson, 1985: On the use and significance of isentropic potential vorticity maps. *Quarterly Journal of the Royal Meteorological Society*, **111**, 877–946, <https://doi.org/10.1002/qj.49711147002>.
- Kalnay, E., and Coauthors, 1996: The NCEP/NCAR 40-Year Reanalysis Project. *Bulletin of the American Meteorological Society*, **77**, 437–471. [https://doi.org/10.1175/1520-0477\(1996\)077<0437:tnyrp>2.0.co;2](https://doi.org/10.1175/1520-0477(1996)077<0437:tnyrp>2.0.co;2)
- Keyser, D., and M. A. Shapiro, 1986: A review of the structure and dynamics of upper-level frontal zones. *Mon. Wea. Rev.*, **114**, 452–499, [https://doi.org/10.1175/1520-0493\(1986\)114<0452:AROTSA>2.0.CO;2](https://doi.org/10.1175/1520-0493(1986)114<0452:AROTSA>2.0.CO;2)
- Kistler, R., and Coauthors, 2001: The NCEP–NCAR 50-Year Reanalysis: Monthly Means CD-ROM and Documentation. *Bulletin of the American Meteorological Society*, **82**, 247–267. [https://doi.org/10.1175/1520-0477\(2001\)082<0247:tnnyrm>2.3.co;2](https://doi.org/10.1175/1520-0477(2001)082<0247:tnnyrm>2.3.co;2)
- Kobayashi, S., and Coauthors, 2015: The JRA-55 Reanalysis: General Specifications and Basic Characteristics. *Journal of the Meteorological Society of Japan*, **93**, 5–48, <https://doi.org/10.2151/jmsj.2015-001>.

- Koch, P., H. Wernli, and H. Davies, 2006: An Event-based jet-stream climatology and typology. *International Journal of Climatology*, **26**, 283–301, <https://doi.org/10.1002/joc.1255>.
- Manney, G. L., and M. I. Hegglin, 2018: Seasonal and Regional Variations of Long-Term Changes in Upper-Tropospheric Jets from Reanalyses. <https://doi.org/10.1175/JCLI-D-17-0303.1>.
- Manney, G. L., and Coauthors, 2011: Jet characterization in the upper troposphere/lower stratosphere (UTLS): applications to climatology and transport studies. *Atmospheric Chemistry and Physics*, **11**, 6115–6137, <https://doi.org/10.5194/acp-11-6115-2011>.
- Manney, G. L., M. I. Hegglin, W. H. Daffer, M. J. Schwartz, M. L. Santee, and S. Pawson, 2014: Climatology of Upper Tropospheric–Lower Stratospheric (UTLS) Jets and Tropopauses in MERRA. <https://doi.org/10.1175/JCLI-D-13-00243.1>.
- , and Coauthors, 2017: Reanalysis comparisons of upper tropospheric–lower stratospheric jets and multiple tropopauses. *Atmospheric Chemistry and Physics*, **17**, 11541–11566, <https://doi.org/10.5194/acp-17-11541-2017>.
- Martin, J. E., 2021: Recent Trends in the Waviness of the Northern Hemisphere Wintertime Polar and Subtropical Jets. *Journal of Geophysical Research: Atmospheres*, **126**, e2020JD033668, <https://doi.org/10.1029/2020JD033668>.
- Martineau, P., G. Chen, and D. A. Burrows, 2017: Wave Events: Climatology, Trends, and Relationship to Northern Hemisphere Winter Blocking and Weather Extremes. <https://doi.org/10.1175/JCLI-D-16-0692.1>.
- McWilliams, J. C., and J. H. S. Chow, 1981: Equilibrium Geostrophic Turbulence I: A Reference Solution in a β -Plane Channel. *J. Phys. Oceanogr.*, **11**, 921–949, [https://doi.org/10.1175/1520-0485\(1981\)011<0921:EGTIAR>2.0.CO;2](https://doi.org/10.1175/1520-0485(1981)011<0921:EGTIAR>2.0.CO;2)
- Miller, R. L., G. A. Schmidt, and D. T. Shindell, 2006: Forced annular variations in the 20th century Intergovernmental Panel on Climate Change Fourth Assessment Report models.

Journal of Geophysical Research: Atmospheres, **111**,
<https://doi.org/10.1029/2005JD006323>.

Morgan, M. C., and J. W. Nielsen-Gammon, 1998: Using Tropopause Maps to Diagnose Midlatitude Weather Systems. *Mon. Wea. Rev.*, **126**, 2555–2579,
[https://doi.org/10.1175/1520-0493\(1998\)126<2555:UTMTDM>2.0.CO;2](https://doi.org/10.1175/1520-0493(1998)126<2555:UTMTDM>2.0.CO;2)

Namias, J., and P. F. Clapp, 1949: Confluence theory of the high tropospheric jet stream. *J. Meteor.*, **6**, 330–336, [https://doi.org/10.1175/1520-0469\(1949\)006<0330:CTOTHT>2.0.CO;2](https://doi.org/10.1175/1520-0469(1949)006<0330:CTOTHT>2.0.CO;2)

Newton, C. W., 1954: Frontogenesis and frontolysis as a three-dimensional process. *J. Meteor.*, **11**, 449–461, [https://doi.org/10.1175/1520-0469\(1954\)011<0449:FAFAAT>2.0.CO;2](https://doi.org/10.1175/1520-0469(1954)011<0449:FAFAAT>2.0.CO;2).

Panetta, R. L. (1993). Zonal jets in wide baroclinically unstable regions: Persistence and scale selection. *Journal of the Atmospheric Sciences*, *50*, 2073–2106.
[https://doi.org/10.1175/1520-0469\(1993\)050<2073:zjiwbu>2.0.co;2](https://doi.org/10.1175/1520-0469(1993)050<2073:zjiwbu>2.0.co;2)

Petoukhov, V., S. Rahmstorf, S. Petri, and H. J. Schellnhuber, 2013: Quasiresonant amplification of planetary waves and recent Northern Hemisphere weather extremes. *Proceedings of the National Academy of Sciences*, **110**, 5336–5341,
<https://doi.org/10.1073/pnas.1222000110>.

Randel, W. J., D. J. Seidel, and L. L. Pan, 2007: Observational characteristics of double tropopauses. *Journal of Geophysical Research: Atmospheres*, **112**,
<https://doi.org/10.1029/2006JD007904>.

Rhines, P. B., 1975: Waves and turbulence on a beta-plane. *Journal of Fluid Mechanics*, **69**, 417–443, <https://doi.org/10.1017/S0022112075001504>.

Röthlisberger, M., S. Pfahl, and O. Martius, 2016: Regional-scale jet waviness modulates the occurrence of midlatitude weather extremes. *Geophysical Research Letters*, **43**, 10,989–10,997, <https://doi.org/10.1002/2016GL070944>.

- Santer, B. D., J. J. Hnilo, T. M. L. Wigley, J. S. Boyle, C. Doutriaux, M. Fiorino, D. E. Parker, and K. E. Taylor, 1999: Uncertainties in observationally based estimates of temperature change in the free atmosphere. *Journal of Geophysical Research: Atmospheres*, **104**, 6305–6333, <https://doi.org/10.1029/1998JD200096>.
- Screen, J. A., and I. Simmonds, 2010: The central role of diminishing sea ice in recent Arctic temperature amplification. *Nature*, **464**, 1334–1337, <https://doi.org/10.1038/nature09051>.
- , and ———, 2013: Exploring links between Arctic amplification and mid-latitude weather. *Geophysical Research Letters*, **40**, 959–964, <https://doi.org/10.1002/grl.50174>.
- , and ———, 2014: Amplified mid-latitude planetary waves favour particular regional weather extremes. *Nature Clim Change*, **4**, 704–709, <https://doi.org/10.1038/nclimate2271>.
- Serreze, M. C., A. P. Barrett, J. C. Stroeve, D. N. Kindig, and M. M. Holland, 2009: The emergence of surface-based Arctic amplification. *The Cryosphere*, **3**, 11–19, <https://doi.org/10.5194/tc-3-11-2009>.
- Shapiro, M. A., and Coauthors, 1999: A planetary-scale to mesoscale perspective of the life cycles of extratropical cyclones: The bridge between theory and observations. *The Life Cycle of Extratropical Cyclones*, M. A. Shapiro and S. Gronas, Eds., Amer. Meteor. Soc., 139–185.
- Shapiro, M. A., and D. Keyser, 1990: Fronts, jet streams and the tropopause. *Extratropical Cyclones: The Erik Palmén Memorial Volume*, C. Newton and E. O. Holopainen, Eds., Amer. Meteor. Soc., 167–191.
- Strong, C., and R. E. Davis, 2007: Winter jet stream trends over the Northern Hemisphere. *Quarterly Journal of the Royal Meteorological Society*, **133**, 2109–2115, <https://doi.org/10.1002/qj.171>.

- Sturaro, G., 2003: A closer look at the climatological discontinuities present in the NCEP/NCAR reanalysis temperature due to the introduction of satellite data. *Climate Dynamics*, **21**, 309–316, <https://doi.org/10.1007/s00382-003-0334-4>.
- Swart, N. C., and J. C. Fyfe, 2012: Observed and simulated changes in the Southern Hemisphere surface westerly wind-stress. *Geophysical Research Letters*, **39**, <https://doi.org/10.1029/2012GL052810>.
- Vavrus, S. J., 2018: The Influence of Arctic Amplification on Mid-latitude Weather and Climate. *Curr Clim Change Rep*, **4**, 238–249, <https://doi.org/10.1007/s40641-018-0105-2>.
- Whitney, L. F., 1977: Relationship of the Subtropical Jet Stream to Severe Local Storms. *Mon. Wea. Rev.*, **105**, 398-412, [https://doi.org/10.1175/1520-0493\(1977\)105<0398:ROTSJS>2.0.CO;2](https://doi.org/10.1175/1520-0493(1977)105<0398:ROTSJS>2.0.CO;2)
- Woollings, T., and M. Blackburn, 2012: The North Atlantic Jet Stream under Climate Change and Its Relation to the NAO and EA Patterns. <https://doi.org/10.1175/JCLI-D-11-00087.1>.
- Xu, J., R. Tian, and S. Feng, 2021: Comparison of Atmospheric Vertical Motion over China in ERA-Interim, JRA-55, and NCEP/NCAR Reanalysis Datasets. *Asia-Pacific J Atmos Sci*, **57**, 773–786, <https://doi.org/10.1007/s13143-021-00226-5>.
- Yin, J. H., 2005: A consistent poleward shift of the storm tracks in simulations of 21st century climate. *Geophysical Research Letters*, **32**, <https://doi.org/10.1029/2005GL023684>.